LATERAL HETEROGENEITY OF BASIN-PLAIN TURBIDITES OF THE CLORIDORME

FORMATION, QUEBEC, CANADA: IMPLICATIONS FOR HORIZONTAL WELL

PREDICTION

by

Chance Seckinger

A thesis submitted to the Faculty and the Board of Trustees of the Colorado School of Mines in partial fulfilment of the requirements for the degree of Master of Science (Geology).

Golden, Colorado

Date _____

Signed: _____

Chance M. Seckinger

Signed: _____

Dr. Zane Jobe
Thesis Advisor

Golden, Colorado

Date _____

Signed: _____

Dr. Wendy Bohrson
Department Head
Department of Geology and
Geological Engineering

ABSTRACT

Facies models for basin-plain turbidite systems often depict very simplistic event-bed geometries that are tabular at the kilometer scale. However, recent studies have demonstrated more complex facies architectures, including rapid changes in event-bed thickness and facies composition. This lateral event-bed heterogeneity can have a significant impact on reservoir prediction, heterogeneity, and production in hydrocarbon reservoirs developed in basin-plain turbidite systems. Coastal outcrops on the Gaspe Peninsula in Quebec expose the Middle Ordovician Cloridorme Formation, a synorogenic 'flysch' turbidite system developed in the Taconic foreland basin. The formation is interpreted to occupy a basin-floor position due to long-distance (10s of kilometers) correlations of bedsets in the direction of current-flow.

This outcrop-based study of the Cloridorme Formation was conducted to better understand the detailed turbidite and hybrid-event-bed architecture in a basin-plain setting. High-resolution drone photogrammetry, centimeter-scale measured sections, digital lithology logs, and handheld gamma-ray scintillometry data characterize this turbidite system at event-bed scales. While most beds in this outcrop study can be traced for 600 meters or more, our results indicate significant intra- and inter-bed lateral complexity, including changes in bed thickness, grain size distribution, and sedimentary structures.

This study provides a framework for event-bed lateral variability in basin-plain settings, using the Cloridorme Formation and other well-constrained outcrop analogs. The quantification of these lateral changes can be used for the management of subsurface heterogeneity in conventional and unconventional hydrocarbon reservoir systems, through reservoir model parameterization and prediction of heterogeneity in horizontal wells.

TABLE OF CONTENTS

LIST OF FIGURES

LIST OF TABLES

ACKNOWLEDGEMENTS

CHAPTER 1

INTRODUCTION

Sediment gravity flow deposits are major targets for hydrocarbon exploration and carbon sequestration, but predicting the lateral heterogeneity and connectivity of reservoir and non-reservoir facies remains a difficult task (Mutti and Normark, 1987; Pyrcz et al., 2005; Jackson et al., 2019; Meirovitz et al., 2020). Variations in stacking patterns, bed thickness, depositional mechanism, grain-size distribution, mineralogy, and sedimentary structures can affect porosity and permeability and, in turn, the potential reservoir volume and connectivity (Sylvester and Lowe, 2004; Pyrcz et al., 2005; Sylvester et al., 2011; Stright et al., 2014; Jackson et al., 2019).

Each sub-environment within a submarine-fan system (e.g., channel, levee, lobe, basin plain) is typically associated with distinct facies, geometries, and bed thickness distributions (Mutti and Normark, 1987; Deptuck et al., 2008; Prélat et al., 2009; Fryer and Jobe, 2019). For example, turbidites deposited in distal basin-plain environments are generally considered to be tabular and 'sheet-like', with laterally consistent facies (Mutti, 1977; Ricci Lucchi and Valmori, 1980; Tőkés and Patacci, 2018). Indeed, long-distance (> 10 km) correlation of individual event beds is possible in some basin-plain settings (e.g., Amy and Talling, 2006; Sumner et al., 2012). However, these studies typically do not measure short distance (< 1 km) variability, which has recently shown to be quite variable even in these settings (Fonnesu et al., 2015; Kane et al., 2017; Baker and Baas, 2020; Spychala et al., 2020), and this heterogeneity is important for incorporation into reservoir models (Lowe et al., 2003; Kvale et al., 2020). In particular, thin (< 20 cm) beds are not often measured or correlated at all, but can be quite laterally variable in

many sub-environments (Hubbard et al., 2020; Fryer et al., 2021; Kus et al., 2021). These thin beds are below the resolution of standard seismic and well-logging tools, so outcrop studies are essential for generating lateral heterogeneity statistics to enable accurate subsurface predictions (Basu and Bouma, 2000). A quantitative analysis of bed-scale heterogeneity within basin-plain turbidites is the focus of this outcrop study.

The Cloridorme Formation, Québec Canada (Fig. 1.1) (Enos, 1965, 1969a, 1969b; Slivitzky et al., 1991) represents a basin-plain turbidite environment, and excellent coastal exposures allow for thin-bedded (< 20 centimeters thick) event beds to be continuously traced for 3 kilometers, and distinct packages of beds to be correlated for 10's of kilometers (Enos, 1969a; Ma, 1996). Several outcrops have been studied in great detail, and bed-by-bed tracing has been used to correlate widely spaced measured sections and note abrupt facies changes (Enos, 1969a; Skipper and Middleton, 1975; Pickering and Hiscott, 1985, 1995; Slivitzky et al., 1991; Ma, 1996; Awadallah and Hiscott, 2004). However, quantitative data for the short-scale lateral heterogeneity of event beds in the Cloridorme remains sparse. This study quantifies the lateral heterogeneity of basin-plain turbidites through a detailed analysis of a well-exposed ~500m wide outcrop of the Cloridorme Formation. We compare our results to previous studies in the Cloridorme Formation, with our high resolution (1-m lateral) measurements revealing much higher bed thinning rates than previously measured. Meanwhile, observed bed continuity and bed thickness appear in-line with other studies, despite the increased resolution of this study. Therefore, predictive models of reservoir properties rely heavily on outcrop analogs as ground-truths for reproducing realistic flow processes and ultimately bed-scale heterogeneity. This study demonstrates the need for more high-resolution studies focusing on vertical and lateral bed-scale relationships to update current conceptual facies models of basin plain environments.
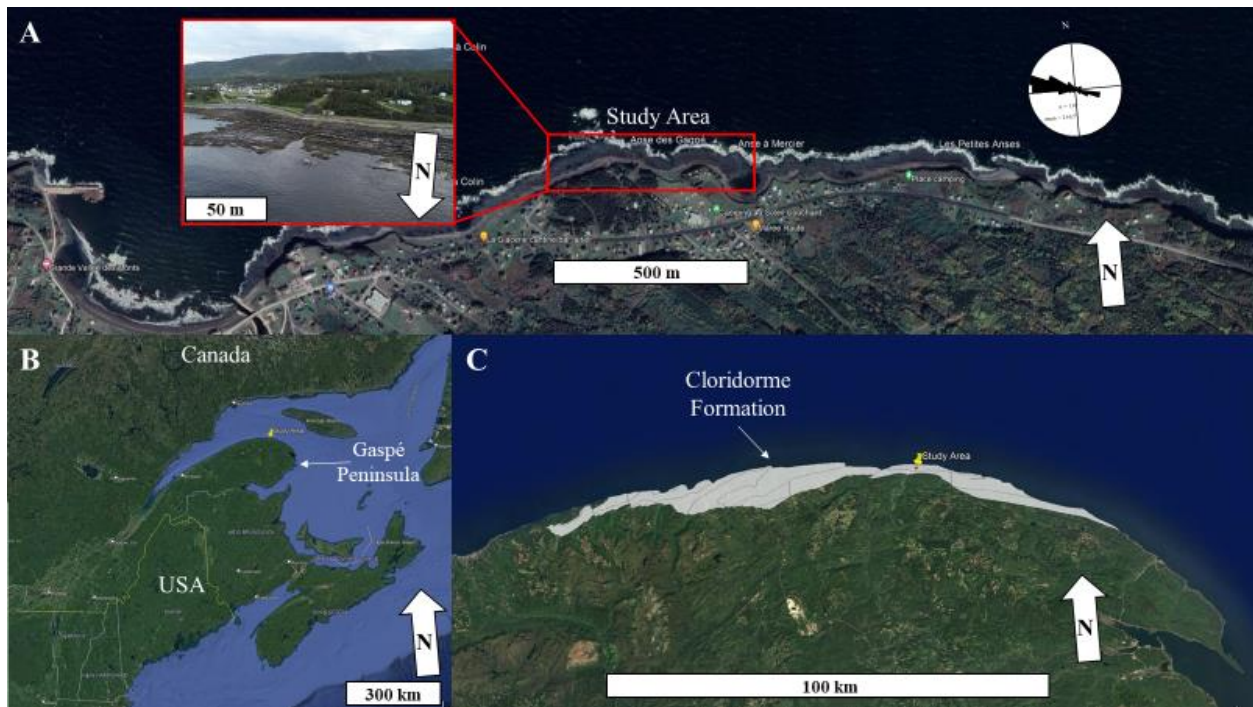
Fig. 1.1   (A) Satellite imagery of the northern coastline of the Gaspé Peninsula, Quebec, Canada. The study area is outlined in red. (B) Satellite view of the Gaspé Peninsula, eastern Quebec, and the northeastern United States. (C) Mapped extent of the Cloridorme Formation, along the northern coastline of the Gaspé Peninsula (after Slivitzky et al., 1991).

CHAPTER 2

GEOLOGIC BACKGROUND

The Upper Ordovician (~450 Ma) Cloridorme Formation is a synorogenic 'flysch' that is exposed along the northern coast of the Gaspé Peninsula, Quebec, Canada (Fig. 1.1) (Enos, 1965, 1969a, 1969b; Slivitzky et al., 1991). The Cloridorme Formation represents a ~ 6,000 m thick submarine-fan system deposited in a foreland basin during the Ordovician Taconic Orogeny (St. Julien and Hubert, 1975; Slivitzky et al., 1991). Graptolite index fossils provide a biostratigraphic framework to constrain the Cloridorme to Middle to Late Caradoc time (c. 456-449 Ma) (Riva, 1968; St. Julien and Hubert, 1975; van Staal, 1994; Fortey et al., 1995; Tucker and Mckerrow, 1995). The early Caradocian Deslandes Formation (*Nemagraptus gracilis* Zone) underlies the Cloridorme Formation which spans the 'impoverished' *Nemagraptus gracilis; Corynoides americanus; Orthograptus ruedemanni;* to *Climacograptus spiniferus* zones (Enos, 1965, 1969a; Fortey et al., 1995; Prave et al., 2000), but due to significant structural deformation, the contact between the two formations is a southwest-dipping thrust fault, making accurate basin reconstruction difficult (Enos, 1969b; St. Julien and Hubert, 1975; Hiscott et al., 1986; Slivitzky et al., 1991). Illite crystal-structure, vitrinite-reflectance data, and the presence of chlorite and sericite minerals in the Cloridorme Formation suggests metamorphism to lower greenschist facies during synorogenic burial (Enos, 1969b; Islam et al., 1982; Tucker et al., 1990). Acadian (Silurian-Devonian) folding and thrusting further deformed the Gaspé region (St. Julien and Hubert, 1975; Hiscott et al., 1986).

While the Cloridorme Formation is structurally deformed, coastal outcrops are locally

very well exposed, and thus many studies have focused on detailed sedimentology. Enos (1965,

1969a, 1969b) used 139 bed correlations over > 3 km to conclude that foreland basin-plain

turbidite successions were much less continuous than hypothesized, a concept that many modern

conceptual facies models still do not employ. Parkash (1970) described downcurrent changes in

sedimentary structures within eight Cloridorme turbidite beds. Hiscott et al. (1986) studied the

Quebec foreland-basin evolution and concluded that the depositional setting of the Cloridorme

transitioned from a flat basin floor (lower 1500-2000m of deposits) to stacked lobe deposits

(middle 2000m) to a muddy lobe-fringe setting (upper 500m of deposits) (Fig. 2.1). Plentiful

paleocurrent measurements (via flute casts, tool marks, ripples, and grain orientations) indicate

dominant paleoflow from east to west/northwest throughout most of the Cloridorme deposition,

with a reversal of flow (towards the southeast) in uppermost strata (Enos, 1965, 1969a; Skipper

and Middleton, 1975; Skipper and Bhattacharjee, 1978; Pickering and Hiscott, 1985).

This study focuses on a 530-meter wide, depositional dip-oriented exposure of the

Cloridorme Formation located 2.3 kilometers northeast of Grande-Vallée, along the Anse des

Gagné bay (49.22938, -65.10589). The outcrops are exposed on the western limb of a slightly

overturned syncline, striking east-west. The beds are overturned by 23 degrees, resulting in beds

dipping to the south at 67 degrees and striking at 273. The overturned nature of the beds

conveniently exposes the bottom of the beds, enabling determination of paleocurrent direction

from flutes and tool marks. Measured paleocurrents indicate westward paleoflow across the

outcrop (Fig. 1.1). Varying stratigraphic subdivisions of the Cloridorme Formation have been

proposed by previous studies (Enos, 1965; Hiscott et al., 1986; Slivitzky et al., 1991). Our study

is focused on a continuously exposed ~50-meter-thick succession that falls within Enos' (1965,

1969a) $\beta 7$ member, group G; Slivitsky's (1991) Gros-Morne member; and Hiscott's (1986) Petite-Vallée Member. This study's outcrop was described by Enos (1969) using two detailed measured sections spaced 735 meters apart (II_4 and II_5) near the west and east sides of the outcrop, from which several beds were also correlated with more measured sections several kilometers to the east. Ma (1996) described and correlated beds across three measured sections (1, 2, and 3W), respectively located near the western edge, the center, and the eastern edge of this study area.
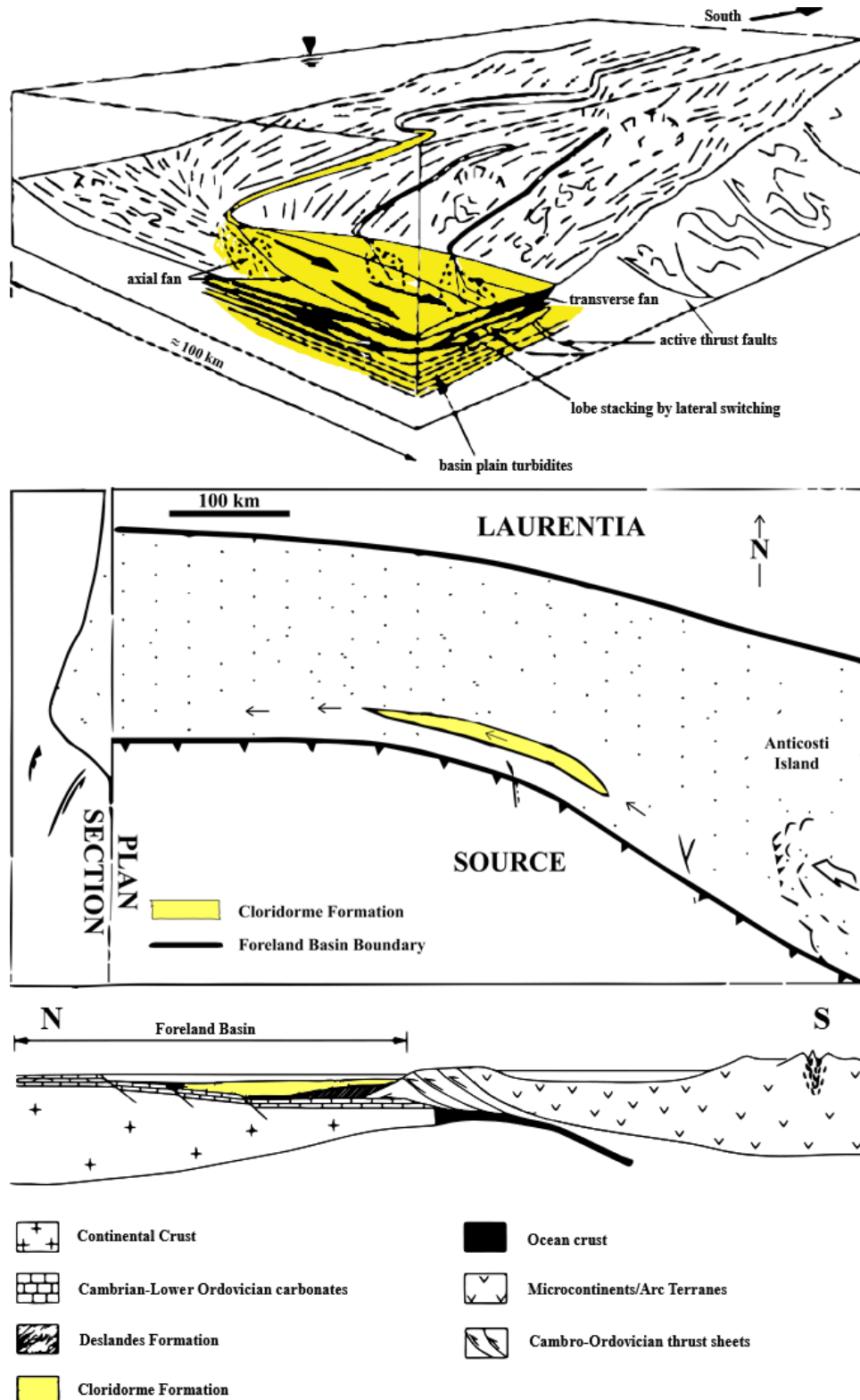
Fig. 2.1   Diagram of foreland basin paleoenvironments during deposition of the Cloridorme Formation (modified from Hiscott et al., 1986; Ma, 1996). The outline of the Ordovician foreland basin was inferred by Hiscott et al. (1986). Tectonic cross-section across the Quebec Appalachians during the Taconic Orogeny modified from Rowley and Kidd (1981).

CHAPTER 3

METHODS

To precisely map and measure the event-bed lateral heterogeneity of the Cloridorme

Formation, a three-dimensional (3D) Digital Outcrop Model (DOM) consisting of 941 drone-

acquired photographs was constructed with Agisoft Metashape (Fig. 3.1). All the photographs

incorporated into this DOM were captured with a DJI Phantom 4 Pro V2 drone. A georeferenced

2-D orthomosaic of the DOM was imported into ESRI ArcMap, where individual bed outlines

were traced and exported as shapefiles to analyze using MATLAB, similar to the techniques

described by Fryer and Jobe (2019) and Kus et al. (2021).

Five stratigraphic sections totaling 430 meters (named MS1 through MS5) were logged at

the centimeter scale and are numbered in ascending order from west to east. Measured sections

were logged to record event-bed boundaries, sedimentary structures, grain size, amalgamation

surfaces, and paleocurrents (Fig. 3.3). Amalgamation surfaces were recognized by abrupt grain-

size changes and scour-features, but we acknowledge that locally narrow grain-size ranges

within a single bed and the weathered outcrop surface may increase uncertainty in identifying

these boundaries. Measured-section data are used to characterize internal architectures present in

sandstone beds and subsequently define distinct facies. The focus of study was to correlate a ~30

m thick interval between sections through physical correlation (i.e., walking out beds in the field)

and tracing using the 3D outcrop model; careful bed-by-bed correlations were made across two

faults (<10 m displacement) (Fig. 3.2). In addition to the detailed measured sections, we

measured six bed-thickness transects – SL1 through SL6 - using an Android app called

'Stratlogger' (https://github.com/jcliang001/Stratlogger) that was developed for this study. These transects help to constrain changes in bed thickness in between detailed measured sections. The measured sections were digitized using the 'StratCoreProcessor' in MATLAB described by Jobe et al. (2021). At MS3, spectral gamma-ray data were recorded every 25 cm with a Radiation Solutions RS-230 handheld gamma-ray spectrometer (90 second data collection window).
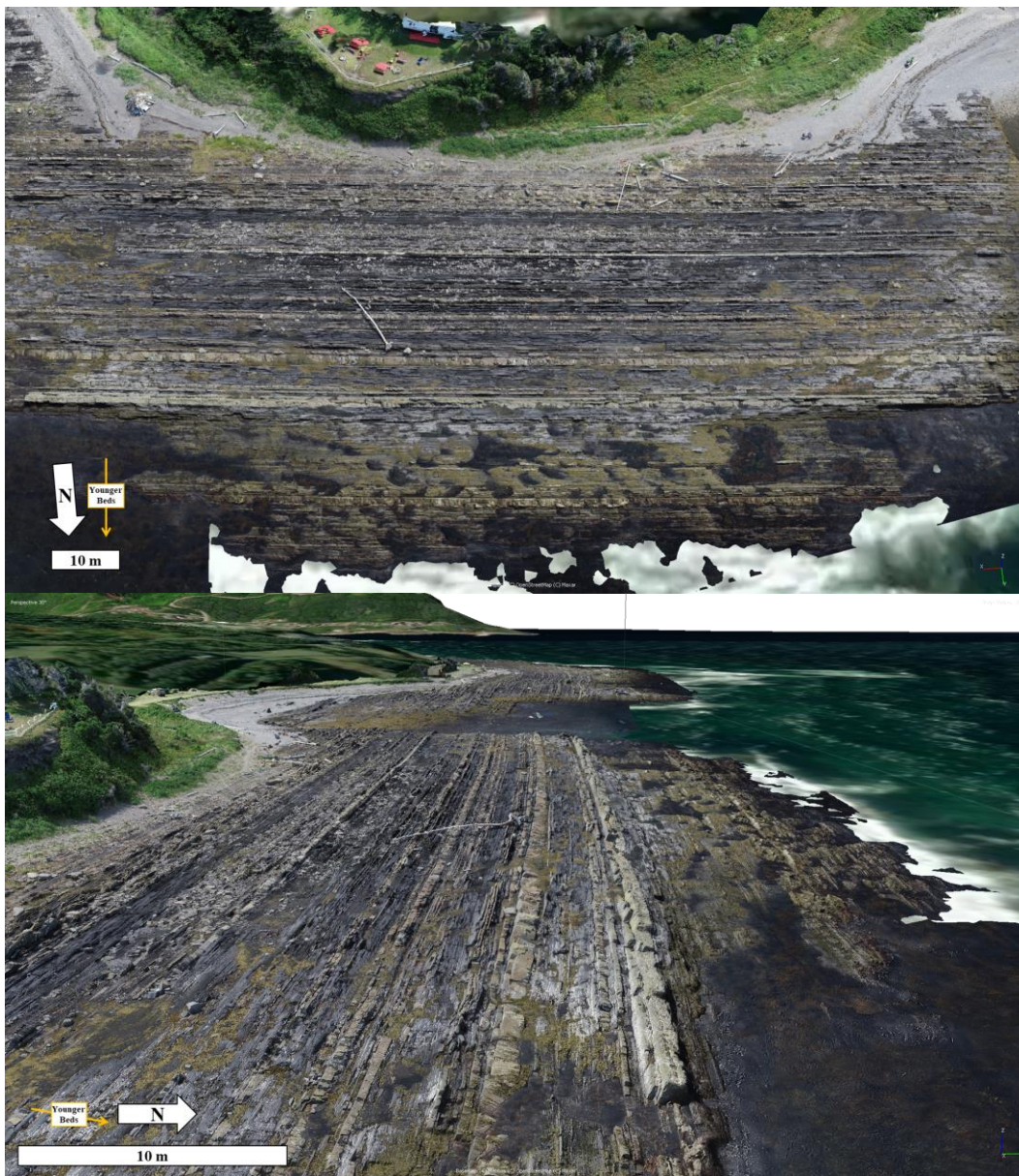
Fig. 3.1   Agisoft 3D DOM constructed from 941 drone images.

Using five graphic logs (MS1-5), this study identifies 85 event beds that are laterally correlable across the outcrop (530 m; Fig. 3.2 and Fig. 3.4). Each event bed was hand-traced along the outcrop and correlated between logs, and later transferred onto a drone-derived orthomosaic. Using MATLAB, we upsampled data from the bed-scale correlations at 1, 10, and 100-m increments for the purpose of comparing (1) lateral variations and (2) sampling intervals across the study area (Fig. 3.5). Although orthomosaics are a powerful tool to view the long-distance lateral continuity of beds, image resolution, variable shoreline, and vegetation obscuring the outcrop face (Fig. 3.1) sometimes present challenges to tracing of event beds on the orthomosaic.

Some authors use the terms 'bed' and 'bed thickness' to refer to the sandstone portion of a turbidite (Carlson and Grotzinger, 2001; Marini et al., 2016), whereas others use bed thickness to refer to the entire sedimentation unit (e.g. total thickness of a sandstone-mudstone couplet; Sylvester, 2007). For the purposes of this study, if not specified otherwise, 'bed' and 'bed thickness' are equivalent to the sandstone portion of a sedimentation unit (i.e., event bed). When considering the sedimentation unit as a whole, the term 'event bed' is used to indicate a sandstone-mudstone couplet that was likely deposited by the same flow (Cf. Fryer and Jobe, 2019). We acknowledge that it is difficult to differentiate the boundary between the mudstone cap of a sedimentation-unit and hemipelagic mud (Cf. Talling et al., 2012; Dall'Olio et al., 2013; Fryer and Jobe, 2019), and so herein we refer to mudstones as an 'interval' rather than a bed. When possible, clearly amalgamated sandstone beds, demarcated by a sand-on-sand contact with abrupt grain size break, were separated into two distinct bed-thickness measurements.
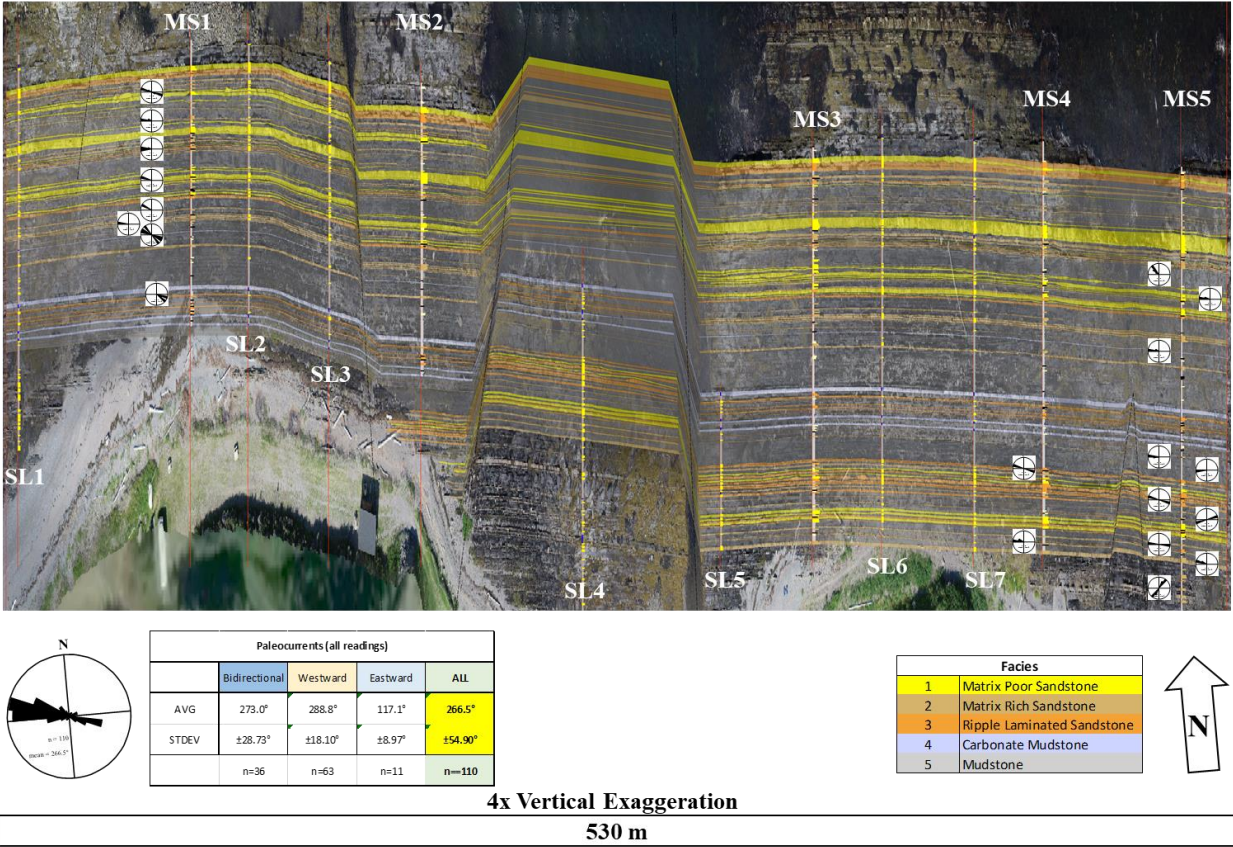
Fig. 3.2   Cross section of detailed measured sections and Stratlogger sections with individual beds traced across the outcrop. Faults are indicated by gray lines transecting the cross section. Bed paleocurrent measurements are shown in their respective locations.
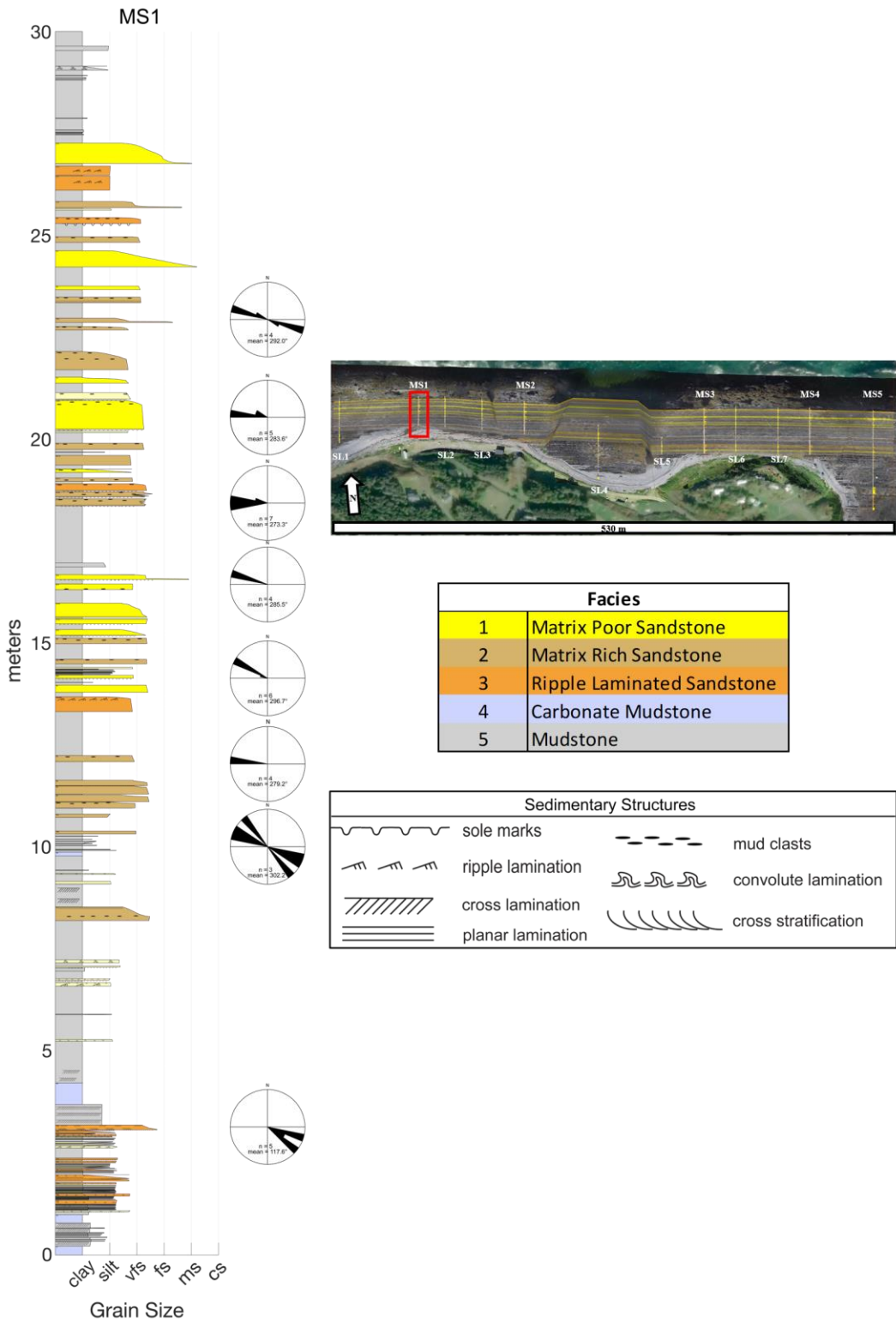
Fig. 3.3   Detailed measured section MS1, with paleocurrent measurements shown in their respective locations.
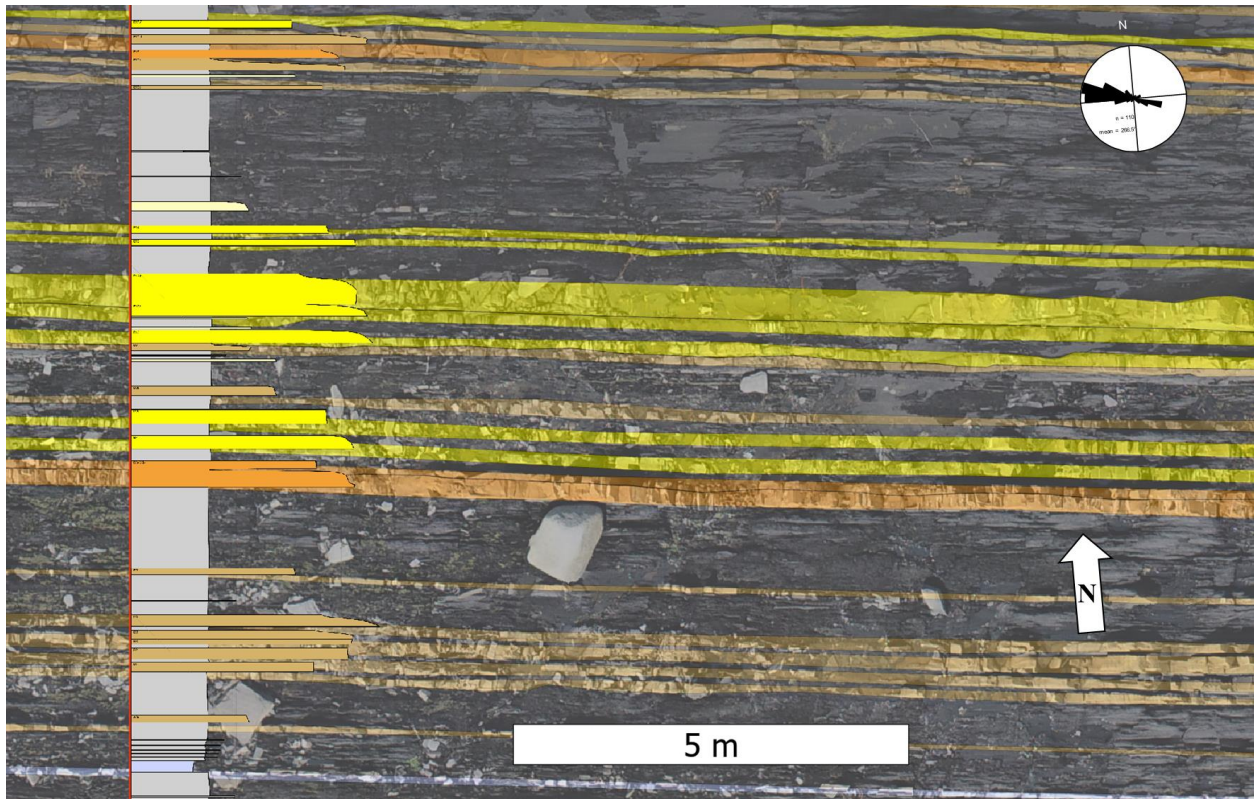
Fig. 3.4   Individual sandstone beds traced on the orthomosaic. Note the slight changes in thickness present in many beds.
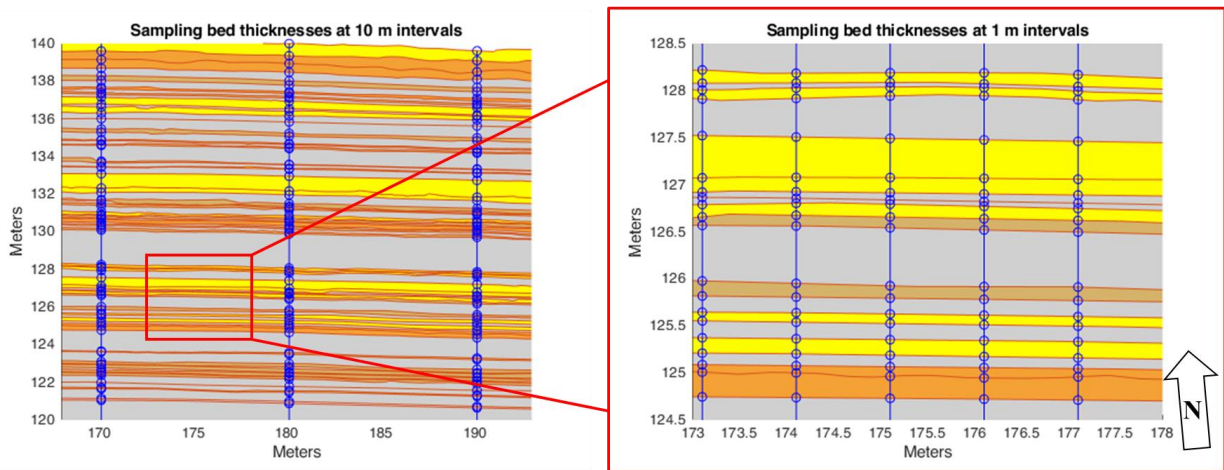
Fig. 3.5   Method for obtaining bed thickness measurements from traced beds at 10 m (left) and 1 m (right) intervals.

CHAPTER 4

RESULTS

4.1   Facies

In this study, the outcrop was initially divided two basic lithologies: mudstone (<63-micron size grains) and sandstone (>63-micron size grains). These lithologies were classified into six facies at the bed scale (described in Table 4.1), which are (1) matrix-poor sandstone, (2) matrix-rich sandstone, (3) ripple-laminated sandstone, (4) carbonate mudstone, (5) mudstone, and (6) ash. The depositional processes for each facies (Table 4.1) were interpreted based on grain size and sedimentary structures. Sandstone facies include matrix-poor sandstones and ripple-laminated sandstones, which include the T_a-T_c divisions deposited by fully turbulent turbidity currents (Bouma, 1962; Lowe, 1982), and matrix-rich sandstone, which includes the H2-H4 divisions of hybrid event beds (HEBs) deposited by "transitional" flows (*sensu* Haughton et al., 2009) resulting from a progressive increase in dispersed clay and dampened turbulence as flows evolve through time and space (Haughton et al., 2009).

Table 4.1   Facies observed in study area, with descriptions of sedimentary structures and inferred depositional processes.

	Facies	Description	Depositional Process	Image
1	Matrix Poor Sandstone	Light tan sandstone, fine to very coarse grains, often normally graded; sparse mudclasts present throughout but more common near the top of beds; sometimes amalgamated.	High-density turbidity current with relatively low clay content (*Bouma Ta; Lowe S3; Haughton H1*).	
2	Matrix Rich Sandstone	Greyish tan clay-rich sandstone, fine to medium grained with some coarse sand grains; typically structureless; mud-clasts abundant in the upper portions of the beds.	Cohesive clay-rich turbidity current (*Haughton H3*).	
3	Ripple Laminated Sandstone	Tan very fine to medium grained rippled sandstone; climbing ripples and convolute laminations common.	Turbidity current with high sedimentation rates; ripples often deformed shortly after deposition (*Bouma Tc*).	
4	Carbonate mudstone	Massive grey to yellow mudstone primarily comprised of dolomite cement and trace detrital silt grains; present as laterally extensive beds or 1-5 m wide lenses. Referred to as 'calcilutite' by some authors	Hemipelagic deposition, with later diagenetic alteration. Likely a condensed interval	
5	Mudstone	Dark grey laminated mudstone; hemipelagic mud with detrital silt grains; fissile. Uncommon thin (1-5 cm) rippled sand beds	Hemipelagic deposition (*Bouma Td-e; Haughton H5*; sand beds are *Bouma* Tc divisions)	
6	Ash	Volcanic ash horizon (bentonite). Laterally correlable over > 5 km (Awedallah and Hiscott, 2004)	Volcanic ash fall deposit	

4.2   Classification of Elements and Complexes

The outcrop was interpreted into a simplified hierarchal scheme comparable to that of Prélat et al. (2009). We identify 12 successions (Elements) of several inter-related event beds and overlying mudstone intervals. The 12 Elements of this outcrop (Element 1 at the base through Element 12 at the top) are comprised of 3 to 11 event beds and range from 1 to 7 meters thick (Fig. 4.1). An Element is interpreted to represent a succession of turbidites stacked to form a submarine lobe element. Multiple Elements stack to form a Complex. A Complex is defined as a group of Elements with similar internal characteristics (i.e. facies types, sand content, and bed thickness), bounded by thick (>2 meter) laterally persistent mudstone intervals. The four identified Complexes (Complex 1 through 4) range from 9 to 12 meters thick and are each comprised of 3 Elements. Each Complex is interpreted as a group of genetically related submarine lobes (Prélat et al., 2009), and intervening mudstone intervals represent a period of widespread hemipelagic deposition.

Vertical changes in stacking patterns are observed in both Elements and Complexes. Individual Elements show distinct compensational stacking patterns that are likely caused by variable seafloor topography during deposition. Overall, the outcrop is dominated by mudstones with interbedded turbidite event beds that are interpreted to be distal ends of submarine lobes, with westward paleoflow directions indicating a depositional-dip exposure. We interpret a distal-to-proximal transition from the base to the top of the outcrop based on increasing bed amalgamation, bed thickness, and sand content (cf. Prélat et al., 2009; Spychala et al., 2017).
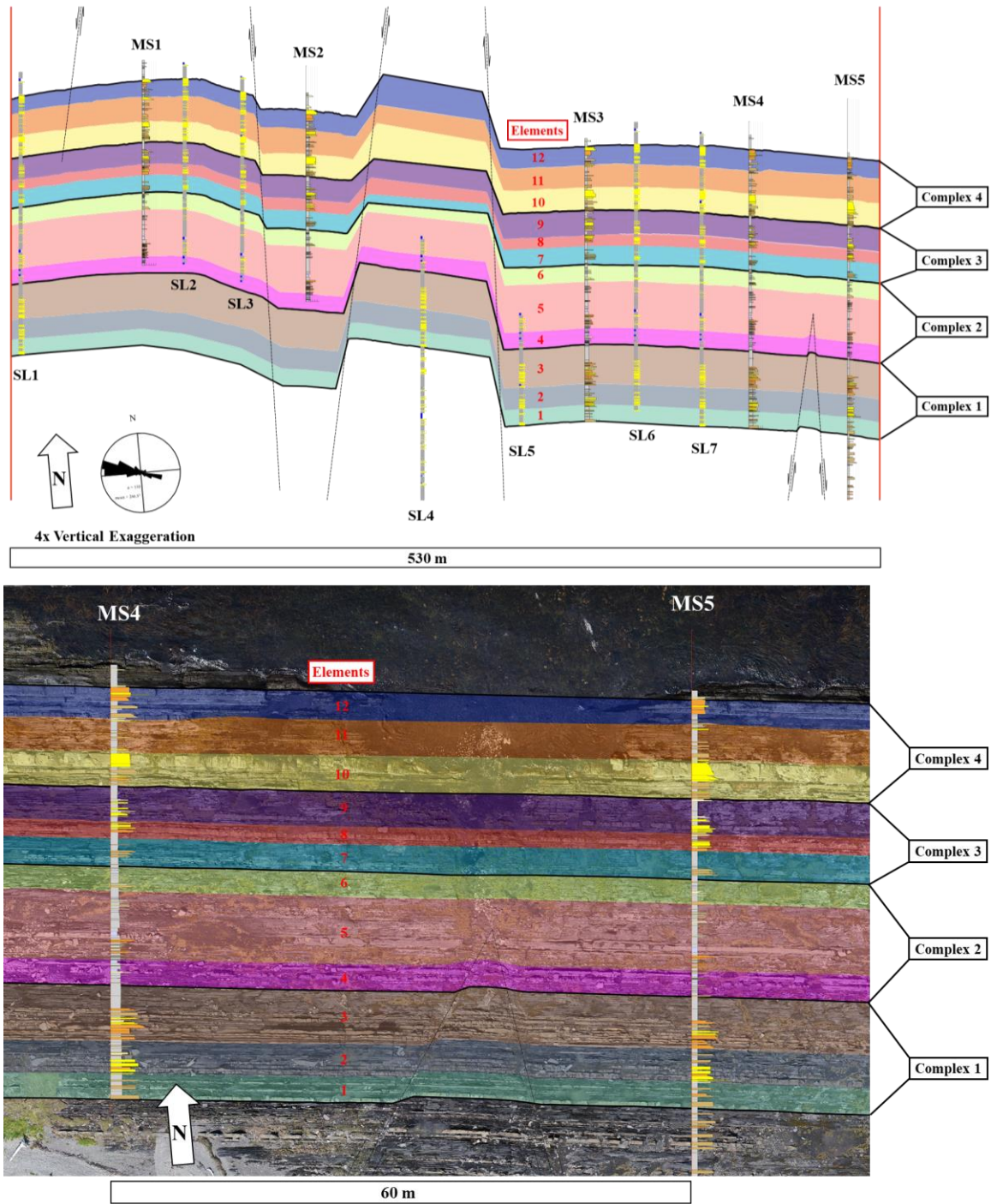
Fig. 4.1   Grouping of 85 beds into 12 Elements and 4 Complexes.

4.3   Quantification of internal characteristics of lobe-elements

4.3.1   *Facies proportion*

Facies proportion (Fproportion) is defined as the thickness of each facies relative to the overall thickness of Element at any location. Stacked bar charts shown in Fig. 4.2 show relative facies proportions for each Element. Fproportion often changes vertically from the base to the top of the outcrop as well as laterally within individual Elements (cf. Kus et al., 2021). The most common facies throughout the outcrop is mudstone (ranging from 65% at MS5 to 71% at MS4). The dominant sandstone facies across most of the outcrop is matrix-poor sandstone, making up the largest proportion of sandstone beds in MS2 through MS5. Matrix-rich sandstone makes up the highest proportion of MS1.

At any one location, Elements tend to have distinct dominant facies and sand content from those vertically stacked below and above; this contrast is less distinct in muddier intervals (e.g., Elements 4 through 7). Elements 10 and 12 are sandy, (e.g. N:G ~0.66) whereas Elements 4, 5, and 6 are muddier (N:G ~0.5 to ~0.13). Muddier elements show less variability in sand facies, compared to sandier elements. For example, muddier Elements 5, 6, and 7 only have one type of sand facies. Each Element exhibits a region of maximum sandiness (e.g. MS3 location for Element 12; MS1 location for Element 5), away from which facies generally become muddier. Element N:G values are listed in Table 4.2, with the highest N:G regions highlighted. The locations of maximum sandiness are not vertically aligned between Elements and can vary laterally by up to ~430m.
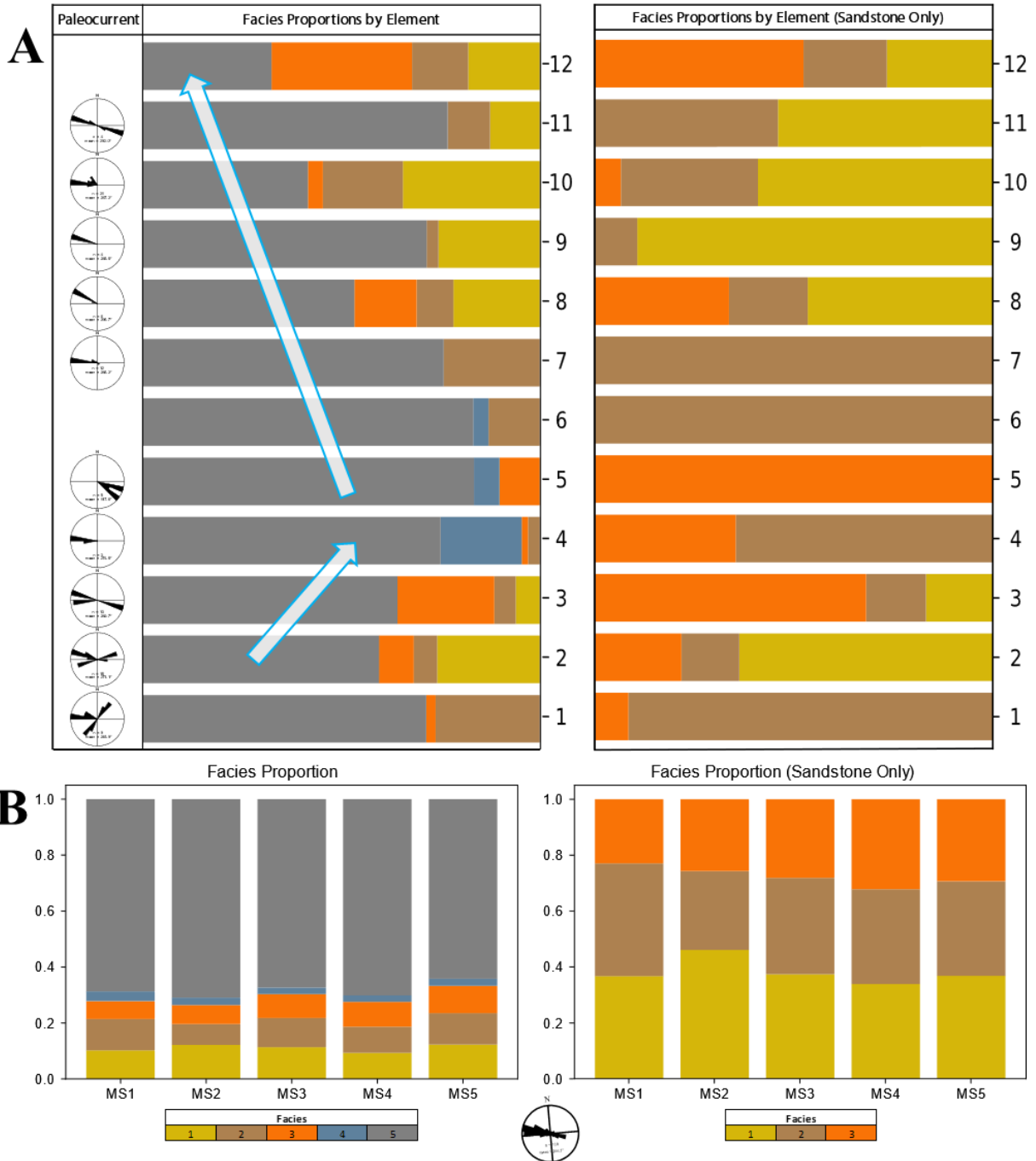
Fig. 4.2   (A) Stacked bar charts showing relative proportion of facies in each Element. (B) Stacked bar charts showing relative proportion of facies at correlated measured sections. See Table 4.1 for facies descriptions.

4.3.2   Net-to-gross

Net-to-gross (N:G) is the ratio of total sand thickness (net) to total stratigraphic thickness (gross) within a defined interval. N:G allows for the comparison of the vertical and lateral changes in sand content, which in turn can inform our understanding of how the depositional system evolved spatiotemporally (e.g. increasing N:G upwards could indicate progradation of the lobe; Macdonald et al., 2011). However, this metric may be less useful for the interpretation of basin plain depositional settings due to the abundance of thin (<10 cm) and non-amalgamated beds. The N:G of elements in the study area ranges from 0.05 to 0.67, with a mean value of 0.33. N:G values at each measured section are listed in Table 4.2, and plotted for the outcrop extent in Fig. 4.3. Elements 1, 2, 3 and 4 were poorly exposed and data was limited to MS3, MS4, and MS5. Elements 5-12 were consistently measured from MS1 through MS5. Overall, N:G increases upward from Elements 1 through 12. Elements 1, 2, 3, 6, 8, 10, and 12 exhibit a trend of overall decreasing N:G from the east to the west. Elements 4, 7, and 11 exhibit increasing N:G from the east to the west. The sandiest (highest N:G) section of each Element varies across the outcrop (highlighted in Table 4.2), suggesting compensational stacking of the Elements.

Table 4.2   Table of Net-to-Gross (N:G) values for Elements at each measured section. The section with the highest N:G is highlighted for each Element, indicating the region of maximum sandiness.

← WEST		← – – –PALEOFLOW– – – –			EAST→	
Element	**MS1**	**MS2**	**MS3**	**MS4**	**MS5**	**AVG N:G**
12	0.62	0.68	0.73	0.69	0.65	0.67
11	0.41	0.25	0.24	0.13	0.27	0.26
10	0.57	0.58	0.63	0.68	0.80	0.65
9	0.30	0.30	0.44	0.20	0.29	0.31
8	0.44	0.47	0.59	0.49	0.54	0.50
7	0.33	0.23	0.22	0.19	0.19	0.23
6	0.16	0.13	0.10	0.11	0.18	0.13
5	0.10	0.05	0.09	0.08	0.09	0.08
4	0.03	0.05	0.05	0.03	0.05	0.04
3	no data	no data	0.35	0.37	0.36	0.36
2	no data	no data	0.37	0.39	0.51	0.42
1	no data	no data	0.29	0.31	0.38	0.33

4.3.3   Amalgamation ratio

Amalgamation ratio (AR) is defined as the number of amalgamation surfaces (i.e. sandstone-on-sandstone contacts) divided by the total number of event beds in a given interval (Romans et al., 2009) and provides insight into flow erosivity. Similar to the patterns observed in N:G, Elements exhibit generally increasing degrees of amalgamation from the base to the top of the outcrop. The average amalgamation ratio across all elements is 0.18 (15 amalgamation surfaces throughout 85 event beds), which suggests that there is an 18% chance that a successive flow will be erosive enough to cause amalgamation. Elements 1, 4, 6, 7, and 11 exhibit no amalgamation surfaces, while Element 12 has the highest average AR at 0.57. Spatial distributions of N:G values, amalgamation ratios, measured event beds, and maximum possible events are plotted in Fig. 4.3.
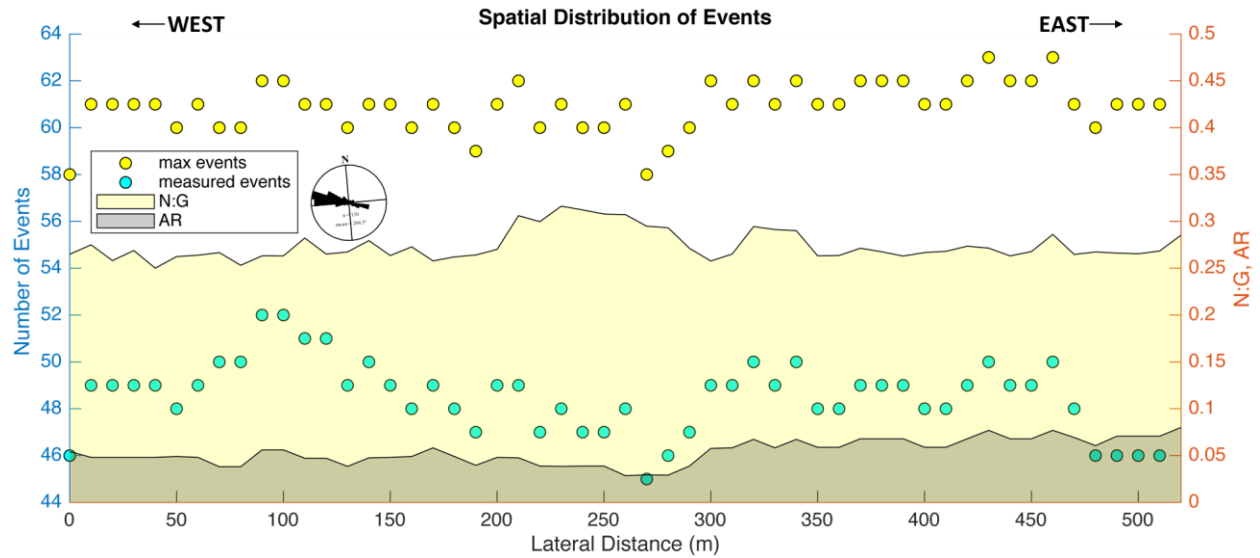
Fig. 4.3   Distribution of measured event beds, maximum possible events, net-to-gross values, and amalgamation ratios of beds traced across the outcrop.

4.3.4   *Stratigraphic Completeness*

It is well known that successive flows can rework or completely erode previous deposits, yet very few studies have tried to quantify the magnitude of how incomplete deep-water deposits are (Vendettuoli et al., 2019). Understanding the number of depositional events that are not preserved is necessary to model the frequency of flows and estimate sedimentation rates in any submarine depositional environment (Jobe et al., 2018). Some scenarios in which a flow's event bed may not be preserved are (but are not limited to): (1) only the muddy tail of a flow is deposited due to bypass of sand, and the muddy tail is indiscernible from the mudstone cap of the previous deposit on which it was deposited; (2) a subsequent flow eroded the underlying sand bed(s), thus erasing the previous depositional event(s); and (3) an amalgamation surface is undetectable to the naked eye due to a limited grain-size range.

Stratigraphic completeness is defined here as the proportion of preserved events (i.e. sand-mud couplets) to the minimum total potential number of events that were deposited in a location (including those not preserved; Durkin et al., 2018; Vendettuoli et al., 2019). For

example, an amalgamated sandstone with a mudstone cap is counted as one preserved event bed and two 'potential events.' Preserved events were plotted against potential events on the scatter plot shown in Fig. 4.4. To calculate the number of potential events, we follow the methods of Kus et al. (2021) and assume that every preserved sandstone bed has an associated mudstone interval that was deposited over the entire study area, regardless of how uniformly the sand was deposited. For example, we assume that if a sandstone bed pinches out, its associated mudstone interval will still be present (and of unchanging thickness) across the entire length of the outcrop. We also make no distinction between hemipelagic and turbiditic mud. Using these assumptions, the mudstone intervals associated with every sandstone bed in the cross section are extended across the entire length of the correlation panel (Fig. 4.5). The effect of this is twofold: (1) mud-on-mud surfaces that are not identifiable in the field (Dennielou et al., 2006) are accounted for in order to calculate the number of potential events at a given location, and (2) the average thickness of mudstone intervals is less than if they were lumped together into one interval. Kus et al. (2021) points out that this method of adjusting the thickness of mudstone intervals, when possible, will also aid in producing more realistic results when calculating mudstone interval thinning rates as compared to lumping multiple mudstone intervals due to indistinguishable mud-on-mud boundaries (cf. Fryer and Jobe, 2019)

At any vertical location, we can compare the number of measured events to the total number of potential events in the cross section to assess the completeness of the stratigraphic record. A positive linear relationship exists between the number of preserved events and the number of potential events. The study area has an average stratigraphic completeness of 82.35%, revealing that less than one-fifth of all sand beds pinch out or are not otherwise preserved in the study area. When compared to submarine lobe deposits of the Point Loma Formation (Kus et al.,

2021), this study shows higher completeness values (Fig. 4.4). This is indicative of a more distal-lobe or basin-plain depositional setting.
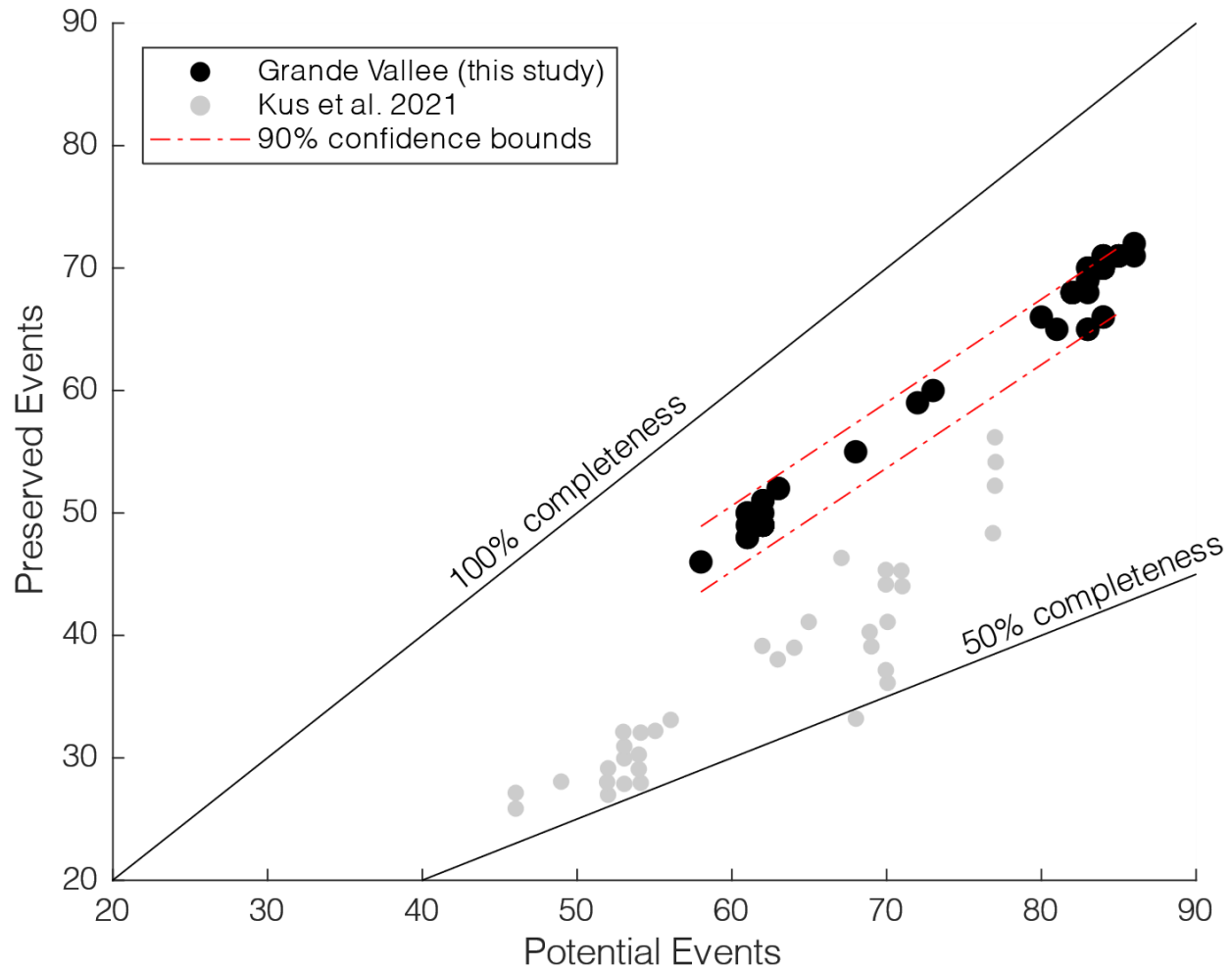
Fig. 4.4   Scatter plot of preserved events (measured event beds) versus potential events (to include beds that pinch out across the outcrop). Points were sampled from the cross section at 20-m intervals. The data is compared to that of Kus et al. (2021).
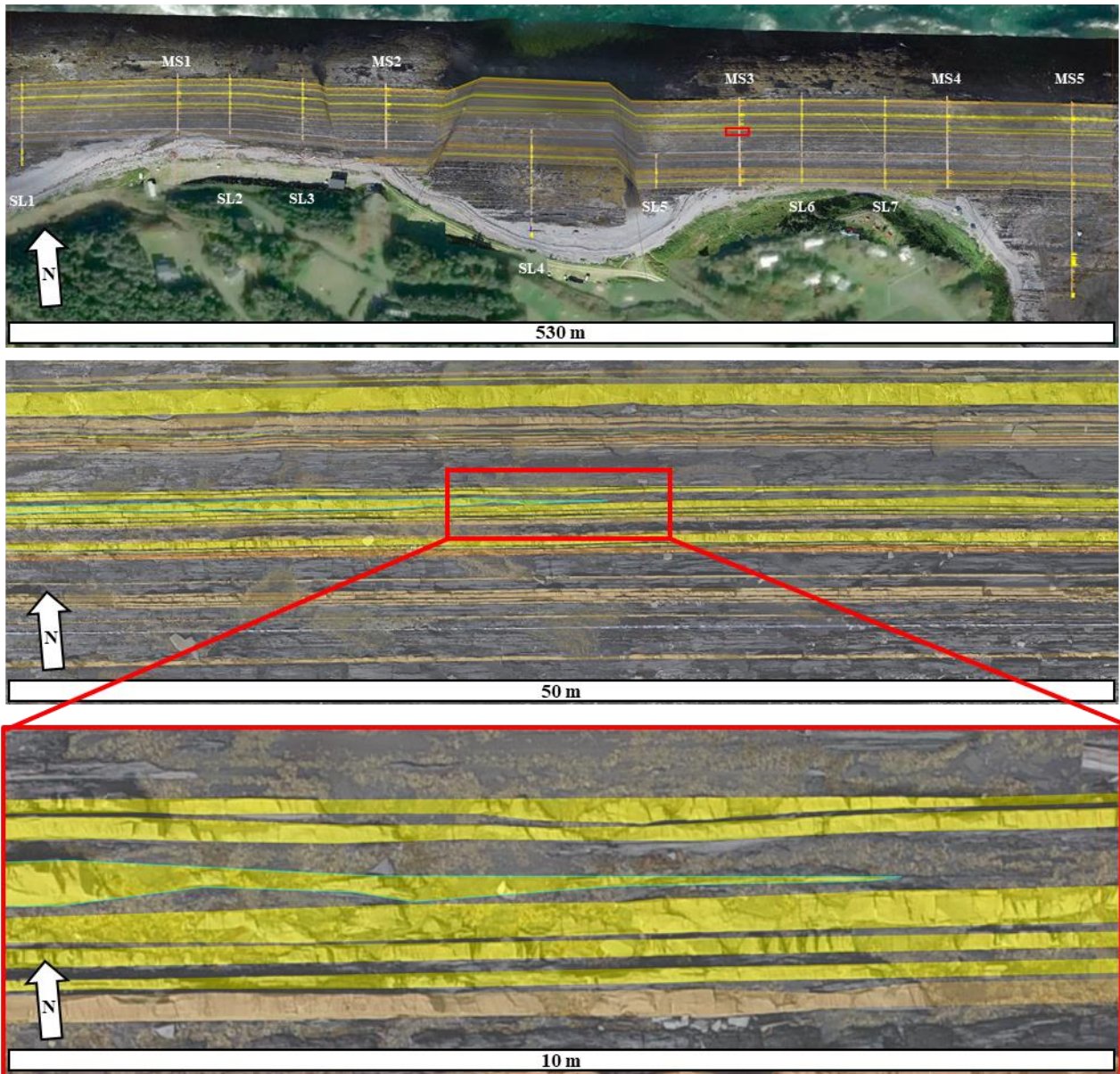
Fig. 4.5   Example of bed-scale correlations between measured sections. A sandstone bed (outlined in blue) is shown pinching out near MS3. Surrounding mudstone intervals are traced across the entire outcrop.

4.3.5   Thickness distribution

Beds display thickness variability between sand and muds, between Elements/Complexes, and between facies. Individual beds also vary in thickness when traced laterally across the outcrop. Generally, mudstone intervals (21 cm median thickness) were thicker than sandstone beds (13 cm median thickness) (Fig. 4.6). Facies 1 (matrix-poor

sandstones) had the highest median bed thickness at 17 cm, followed by Facies 2 (matrix-rich

sandstones) at 12 cm, and Facies 3 (ripple-laminated sandstones) at 11 cm (Fig. 4.6 and Fig. 4.7).

Basin plain elements and complexes also had distinct bed thicknesses. Bed thickness data for

each Element and Complex is presented in Table 4.3.
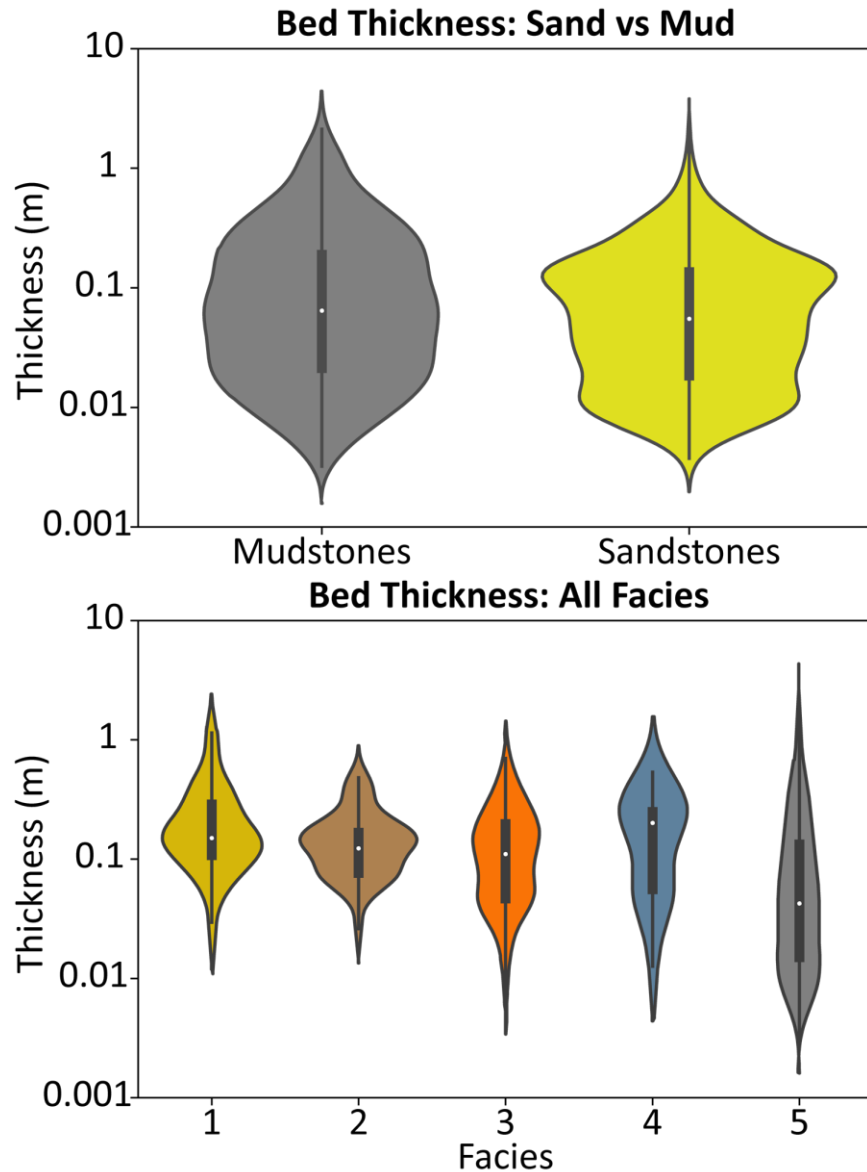
Fig. 4.6   Bed thickness distribution for all mudstones and all sandstones (top), and all facies
(bottom), from measured section data.

4.3.6   Bed thinning rate

Bed thickness and lateral distance can be used to calculate bed-thinning rate (TR_b) by dividing the difference in bed thickness between two nodes by the distance between those nodes (Fryer and Jobe, 2019); for this metric, bed thicknesses are upsampled from the cross section (Fig. 3.2) at 1-m intervals, similar to the methods of Kus et al. (2021). TR_b was calculated such that positive values indicate thinning to the west (downstream) and negative values indicate thinning to the east (upstream); however, we use absolute thinning rate when reporting TR_b because it allows for easier comparison of descriptive statistics (Tőkés and Patacci, 2018). The 10th to 90th percentile range (P_{10} – P_{90}) of TR_b of all sandstone beds is 4.78×10^{-4} m/m to 2.95×10^{-2} m/m and the median thinning rate of all sand beds is 5.41×10^{-3} m/m (Fig. 4.7.). In general, sandstone beds exhibit a wider range of thinning rates than mudstone intervals, which have a P10 to P90 range of 8.22×10^{-4} m/m to 2.85×10^{-2} m/m. The median TRb of all mudstone intervals is 6.94×10^{-3} m/m.
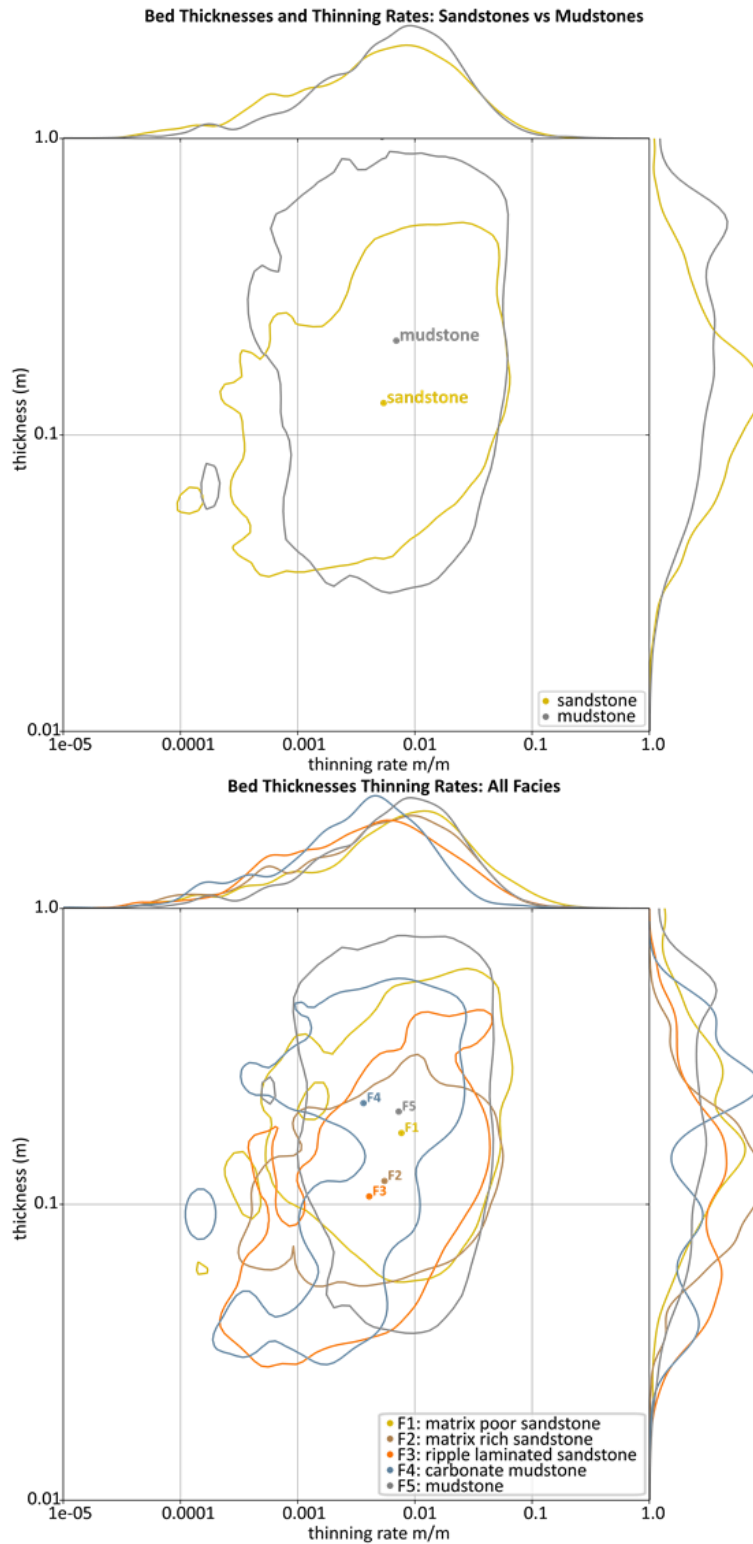
Fig. 4.7   Bivariate kernel density estimate (KDE) plots displaying thinning rates and thickness distributions of each facies. Bed thickness and thinning rate 90% contours are shown. The median for each facies is plotted as a point.

28

4.3.7 Element thinning rate

Element thinning rate (TR_e) is the rate at which an element thins to the west. It is calculated in the same way as bed thinning rate, and a positive value indicates westward thinning. Thinning rates were calculated every 1 m from the cross-section (Fig. 4.1). Lobe-elements thin at significantly higher rates than individual beds, with the average TRe across all elements being 0.0094 m/m (i.e., ~1 m per km). TRe ranges from 0.0043 m/m to 0.0165 m/m. All elements thin to the west. Data for thinning rates by element are shown in Table 4.3.

Table 4.3   Thickness and thinning rate data for each Element and Complex.

Complex	Element	Median Thickness (m)	Median Thinning Rate (m/m)	East to West Ends Thinning Rate (m/m)
	12	2.87	1.50E-02	7.19E-04
4	11	3.59	1.54E-02	8.50E-05
	10	3.50	1.65E-02	1.51E-03
	9	3.46	1.22E-02	4.65E-04
3	8	1.77	1.01E-02	3.23E-04
	7	2.79	6.70E-03	5.57E-04
	6	2.56	6.43E-03	9.28E-05
2	5	7.05	4.92E-03	2.45E-04
	4	2.55	7.80E-03	7.56E-04
	3	5.80	8.93E-03	1.41E-04
1	2	3.19	4.28E-03	9.20E-04
	1	2.53	4.52E-03	3.29E-04
	AVG	3.47	9.40E-03	5.12E-04

CHAPTER 5

DISCUSSION

5.1 Impact of measurement interval on thinning rate calculations

This study demonstrates that while some beds generally remain consistent over the extent

of the outcrop and display very low thinning rates when calculated over hundreds of meters,

most sandstone beds also experience pronounced thickness changes at some point laterally.

Studies that rely upon thinning rates in order to compare sub-environments (Tőkés and Patacci,

2018; Fryer and Jobe, 2019) therefore may unintentionally miss the potential variability in the

system due to constraints of scale and the fidelity of measurement (also discussed by Kus et al.,

2021). We show that the distance over which thinning rates are measured (1 m, 10 m, 100 m) can

impact calculated values by several orders of magnitude. Bed thinning rate empirical cumulative

distribution function (CDF) plots (Fig. 5.1) show this variability in thinning rate. For instance,

when the thickness and thinning rate data from the traced beds sampled at 1-m increments are

plotted against the same beds at 10-m and 100-m increments, we find that there is a significant

shift in the median absolute thinning rate between the two groups. Increasing the sample interval

tends to result in decreased thinning rates (Fig. 5.2). Conversely, there is no significant

difference in bed thickness distributions between different sample intervals. Multiple overlain

bivariate KDE plots display the impact of variations in sample interval distance on bed thickness

and thinning rates (Fig. 5.2).

The data collected by this study is also compared to bed correlations performed by Enos,

1969 that were based on much more widely spaced measured sections. Enos correlated beds

30

between five detailed measured sections spread across 3,015 meters, with spacing intervals ranging from 447 meters to 1,304 meters. Two of those measured sections (II_4 and II_5) span this outcrop and are spaced 735 meters apart. Despite measurements being derived from the same outcrop, thinning rate data derived from Enos (Enos, 1969b, 1969a) is 10-100 times lower than data derived in this study, while bed thickness distributions were not significantly different (Fig. 5.1 and Fig. 5.2).
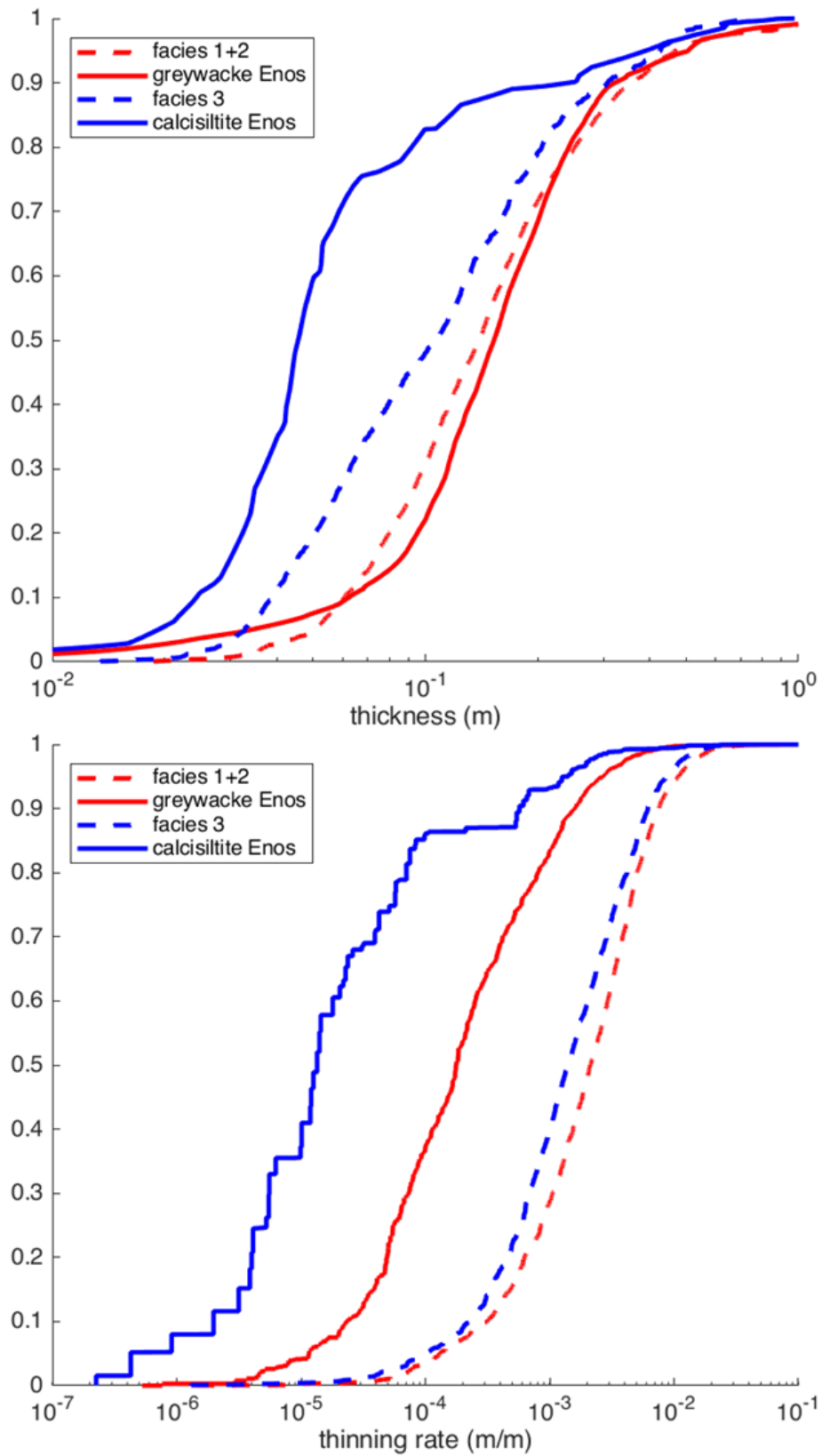
Fig. 5.1   Bed thickness and thinning rate distributions compared to previous work by Enos, 1969.
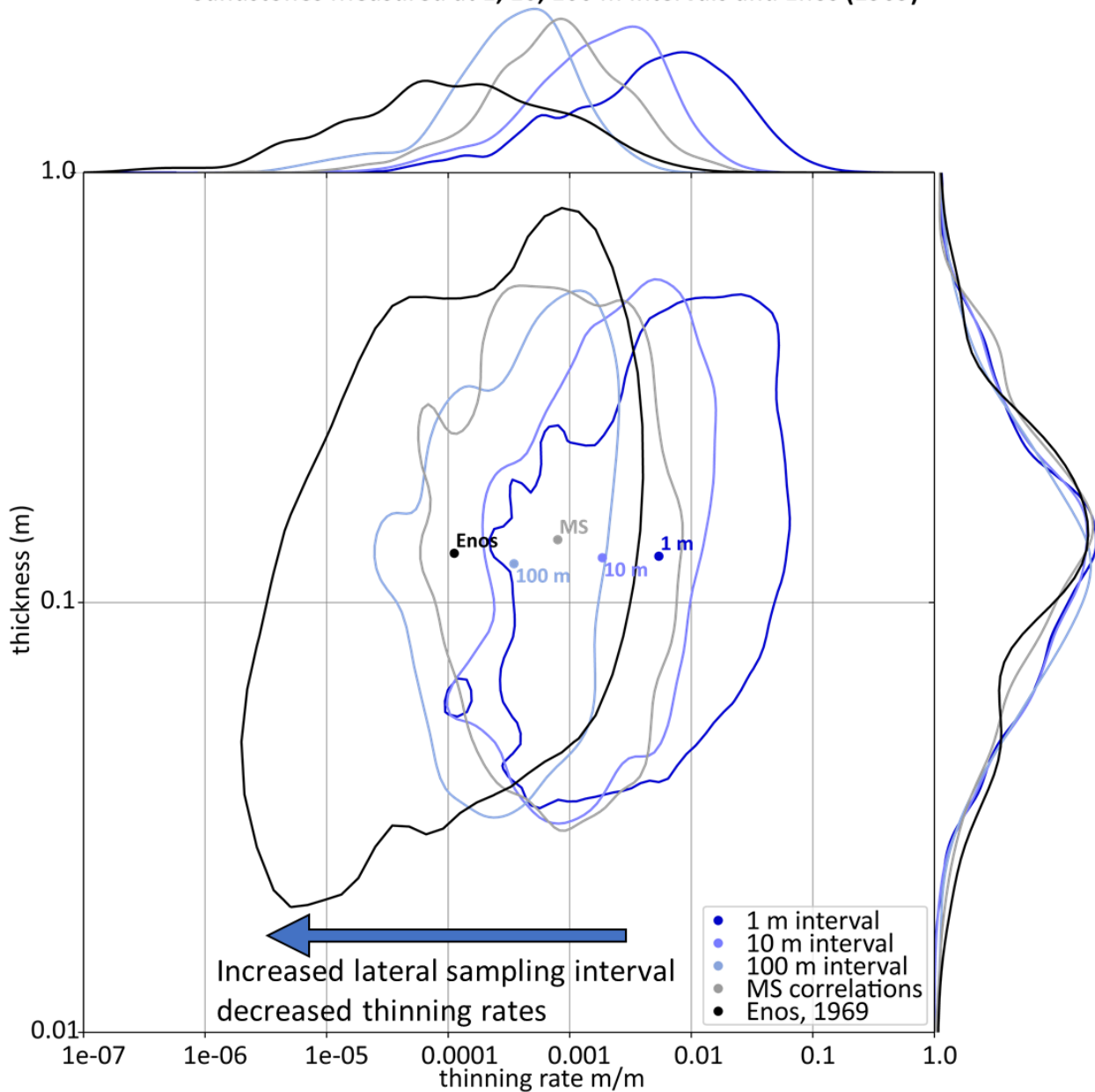
Fig. 5.2   Bivariate KDE plot displaying the impact of sample interval distance on bed thickness and thinning rates. Bed thickness stays the same despite sample interval size, while thinning rate shows higher values with smaller sample intervals. The plotted data for the 100-meter sampling interval most closely aligns with measured section correlations.

5.1.1   Horizontal Sadler effect

The Sadler effect describes variation in apparent sediment accumulation rates and

stratigraphic completion across different time spans and environments of deposition. (Sadler,

1981). The effect states that thicker and more ancient packages of sediment in the stratigraphic

record will record slower sedimentation rates. It also shows that sections are less complete when

measured at shorter timescales. This effect provides a framework for interpreting vertical

changes in stacking patterns, but the principles may also be applicable to investigations of lateral

thickness changes. The beds of this outcrop study represent a relatively short segment of

deposition compared to others of the Cloridorme (e.g. Enos, 1969b and Ma, 1996). Thus, this

study is inferred to encompass a shorter timescale and is less stratigraphically complete than

those of greater magnitude.

5.2   Impact of outcrop orientation on thinning rate calculations

Generally, sand bodies deposited in submarine depositional environments (channel,

levee, lobe) are elongate in shape, with the longest axis corresponding to the depositional dip

direction. Conversely, a depositional strike-exposure would generally show a more compact

sandstone body. This is important to consider when calculating and comparing thinning rates,

because a strike-oriented outcrop will often have higher thinning rates than a dip-oriented

outcrop of the same deposit. The majority of paleocurrent measurements at this outcrop display

dominant westward paleoflow direction. Thus, the east-west oriented beds of this study represent

deposition in the dip direction, and are likely to display lower thinning rates than a strike-

oriented outcrop from the same system.

5.3   Refining depositional environment

The strata of the Cloridorme Formation were previously interpreted as having been

deposited in a submarine fan environment along the axis of a foreland basin (Enos, 1969b;

Beeden, 1983; Hiscott et al., 1986; Ma, 1996), and our findings support this interpretation.

Paleocurrent trends of this study are aligned with the inferred axis of this basin. Bed thinning

rates, bed continuity, and N:G values of this outcrop are most comparable to the "moderately confined" systems of Tőkés and Patacci (2018). Abundant hybrid-event beds (cleaner-lower and muddier-upper) and mud-clasts present in the upper portions of sandstones suggest that the study area occupied a relatively distal position in a confined system (Hodgson, 2009; Talling, 2013; Fonnesu et al., 2015; Malgesini et al., 2015; Kane et al., 2017). We compared the bed thicknesses and thinning rates from within the study area to those reported by Fryer and Jobe (2019), who used a large database with bed-scale data from a variety of submarine sub-environments (Fig. 5.3), including channel, levee, channel lobe transition zone, lobe, and basin plain environments. The Grande Vallee study area has lower bed thicknesses and much higher thinning rates than seen in previous studies of basin plain environments, and as discussed earlier, we observed higher thinning rates than previous studies on the Cloridorme Formation. These discrepancies in thinning rates can be attributed to (1) our very short-scale bed thickness measurement intervals and (2) a general lack of quantitative measurement data for basin plain environments. Measured N:G values, stratigraphic completeness, and amalgamation ratios indicate a distal or fringe position for Elements 1 through 7. Sections with higher N:G and more amalgamation (Elements 8, 10, and 12) indicate the transition to a more proximal or axial position.
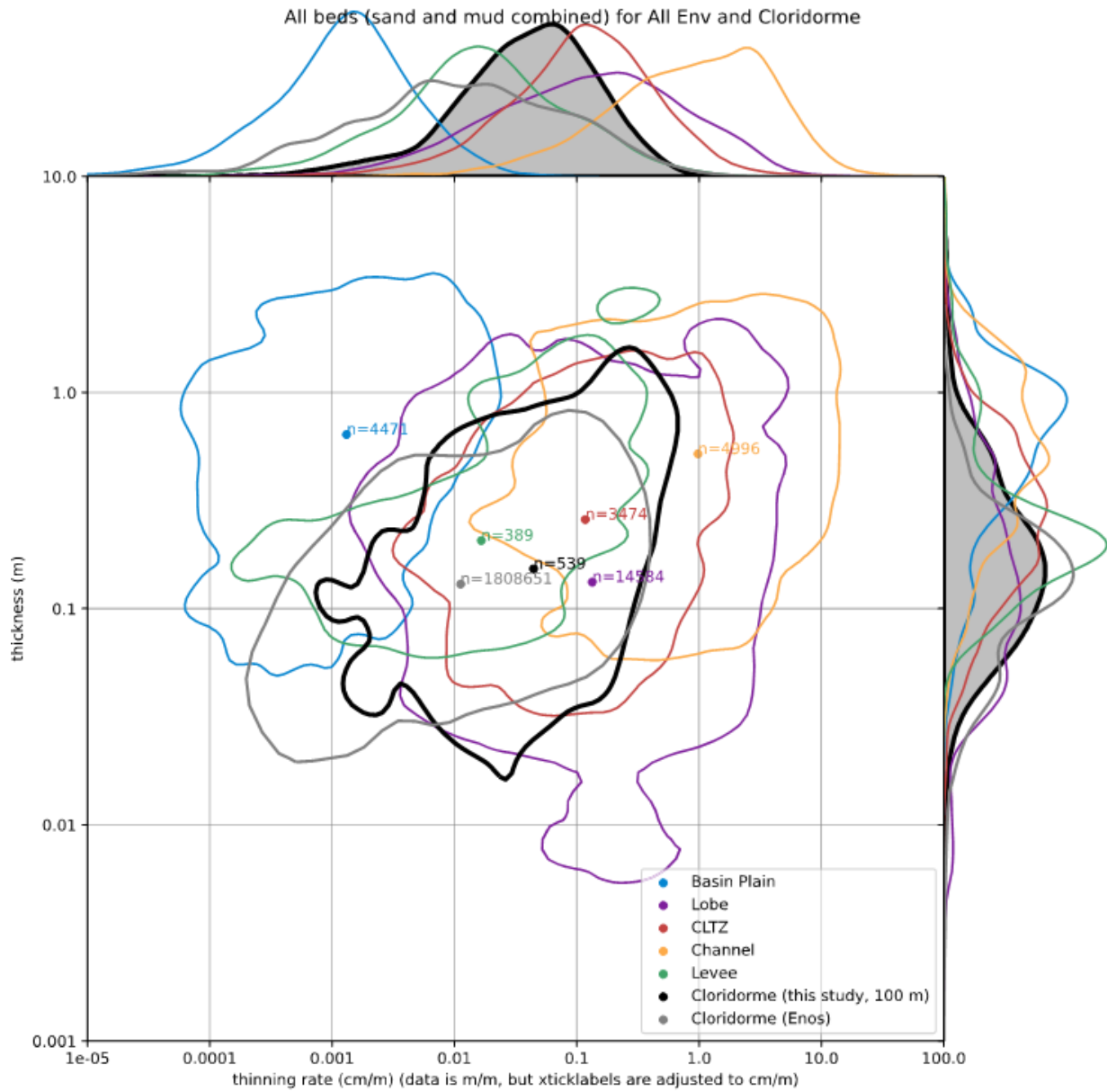
Fig. 5.3   Thinning rate and thickness data from this outcrop plotted with other marine depositional environments from Fryer and Jobe (2019).

5.4   Depositional processes

The bed is the most fundamental building block, upon which the blueprints for reservoir heterogeneity are defined in a deepwater depositional system. The hierarchical relationships between different orders of architectural elements suggest that any heterogeneity at the bed scale is likely to be compounded at larger scales. Therefore, it is crucial to quantify lateral

heterogeneity at the bed-scale to better understand the system. We interpret rapid bed-thickness

changes, sometimes leading to the complete loss or pinch-out of a bed, to indicate that sand beds

are not tabular but are instead deposited irregularly. Four mechanisms for rapid bed-thickness

changes are proposed based on our field observations of bed contacts, primary structures, and

bed continuity away from the thickness change; (1) local scours subsequently filled by coarser-

grained sand, resulting in amalgamation surfaces; (2) variations in basin-floor topography; (3)

transitional flow evolution, resulting in HEBs; and (4) bedforms developed in the base of

turbulent flow (Fig. 5.4). HEBs are known to exhibit rapid lateral facies changes, in which the

lower sandstone portion of a bed pinches out and is replaced by muddier facies before again

becoming sandstone-dominated (Sumner et al., 2009; Fonnesu et al., 2015).

Not all rapid thickness changes preserve clear evidence as to the underlying depositional

process by which the change was produced; moreover, a single bed may be affected by multiple

processes as a flow evolves. Therefore, the case-by-case nature of these observations makes

them very difficult to generalize across even a <1-km study area; also, such high-resolution bed-

scale variability is nearly impossible to identify in the subsurface. These rapid thickness changes

and pinch-outs are commonly subtle because the overall thickness of the strata around the sand

bed remains relatively constant. Detailed tracings of beds from orthomosaics reveal that

sandstone bed thickness within an element is quite variable, even over relatively short distances.

The cumulative effect of multiple rapid bed-thickness changes and pinch-outs at various lateral

and stratigraphic positions—which individually may seem insignificant at the bed scale—

compound to create element-scale variability in overall sandiness. Changes in N:G due to the

cumulative effect of sandstone thickness variability as well as the bed-scale complexity may

greatly impact reservoir properties over short length-scales in lobe deposits. In this outcrop, N:G

values at each measured section ranged from 0.27 (MS2) to 0.34 (MS5). From MS5 to MS4

sandiness decreased most rapidly (5% decrease in sand content over 60m distance). This dataset

can be used to better predict lateral heterogeneity in the subsurface, leading to improved

horizontal well planning and geosteering operations, as well as reservoir model parameterization

from sparse data (e.g. core).
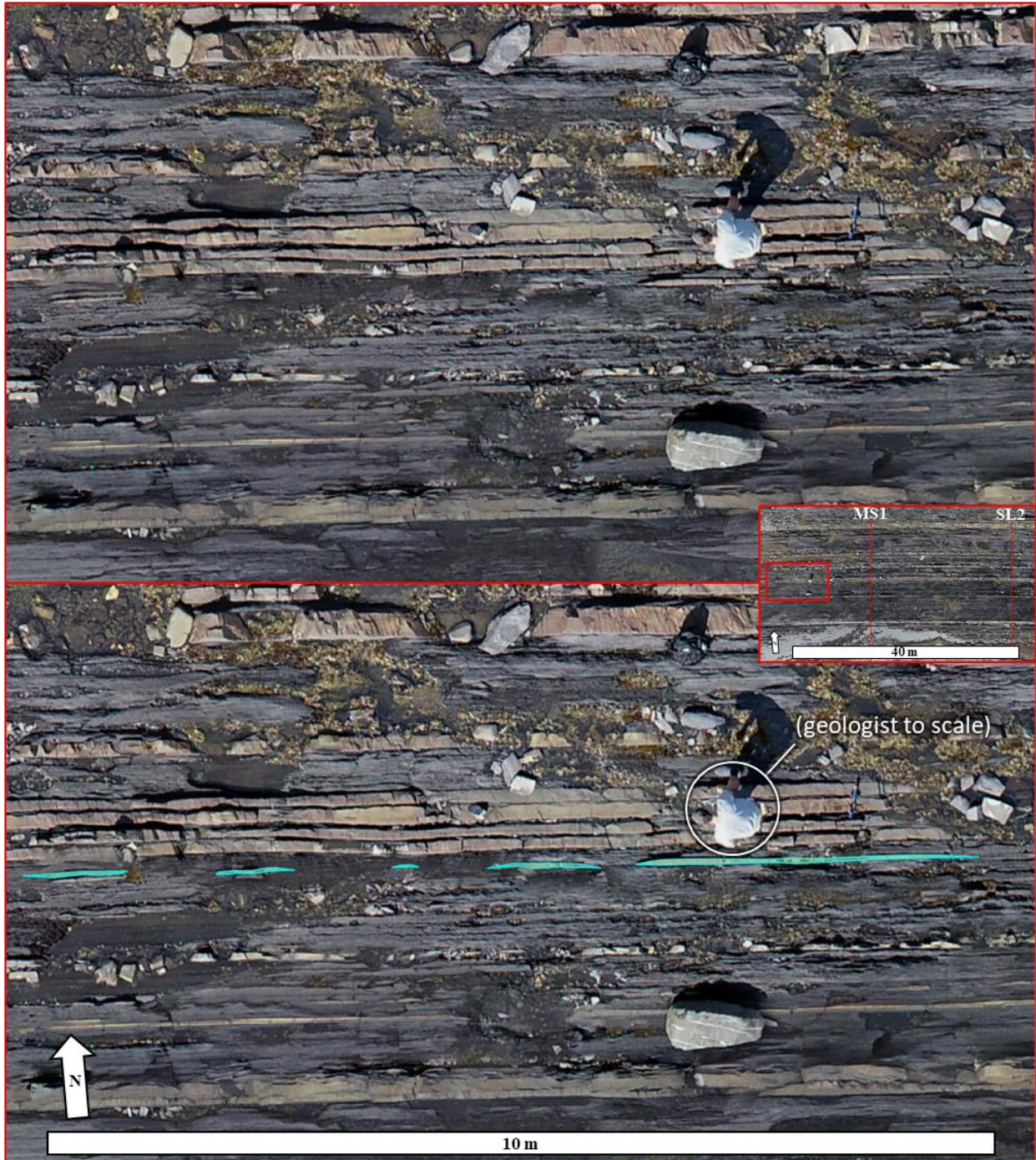
Fig. 5.4   Sandstone bed highlighted in blue in the lower picture showing rapid changes in bed thickness over a short distance (10 meters). Some beds appear to thin and thicken with some regularity. Inset box on the right shows the image in relation to MS1 and SL2.

5.5   Implications for horizontal well prediction

The geometry and stacking of reservoir and non-reservoir facies controls fluid flow due to the presence of permeability barriers and baffles. The lateral-continuity is particularly important when exploring in unconventional reservoirs, where most wells are drilled and completed horizontally, quasi-parallel to bedding. Increasing the efficiency of completions in horizontal wells is an important concern in the oil and gas industry. Horizontal wells are stimulated by injection through clusters of holes ("perforations") in the casing that connects the well to the surrounding formation. Typically, stimulation takes places in stages, with the intention for multiple perforations to be stimulated simultaneously as a part of a single stage (Cheng and Bunger, 2019). Rock quality lateral variations in horizontal wellbores have been shown to be key factors in optimizing hydraulic fracture spacing in unconventional reservoirs. Specifically, heterogeneity along the length of a horizontal well has been shown to impact the propagation of fractures from the clusters in a stage (Manchanda et al., 2016).

Outcrop data from the Cloridorme Formation can be applied to inform production decisions in oil-producing reservoirs like the Bone Spring and Wolfcamp Formations of the Delaware Basin. These formations are heterogeneous in both lateral and vertical directions, and an understanding of the geological complexity is critical for optimizing exploitation strategies. This study provides evidence for increased short-scale lateral heterogeneity in basin plain depositional environments. Fig. 5.5 shows an idealized comparison of lateral heterogeneity and the impact of bed thinning rates on well continuity.
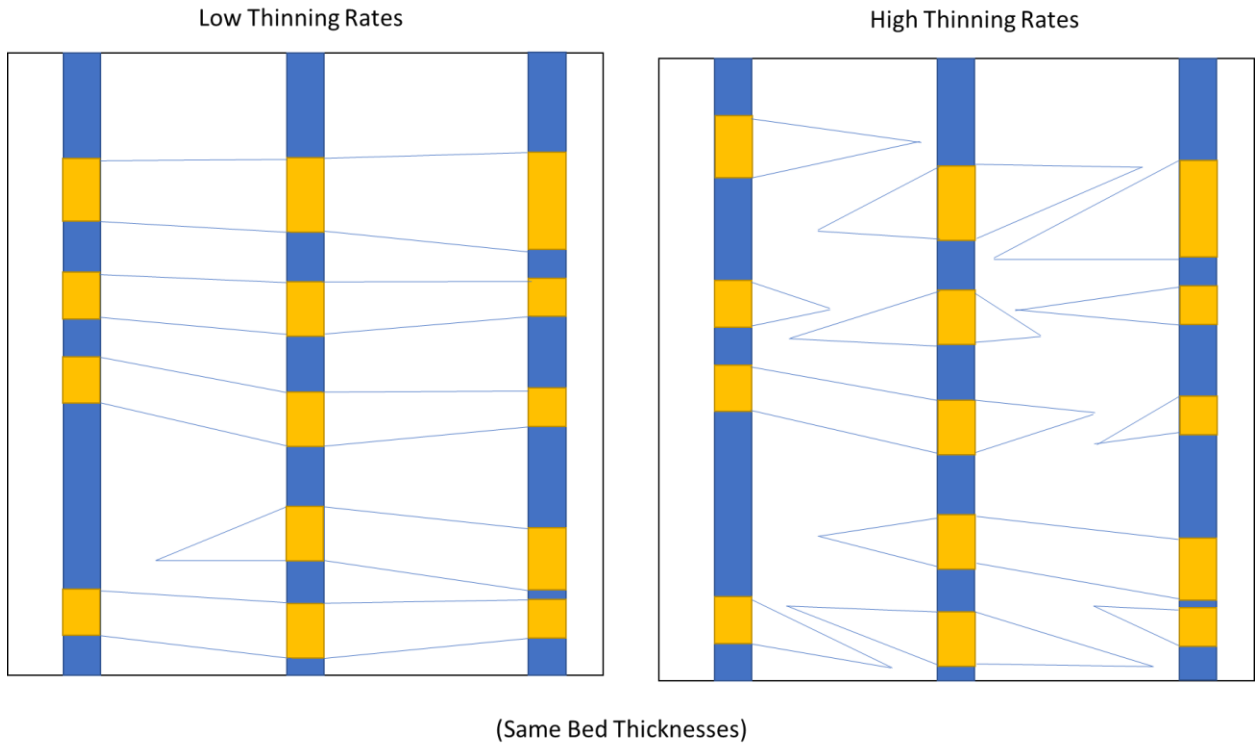
Fig. 5.5   Comparison of low vs high thinning rates and the impact on reservoir continuity.

CHAPTER 6

CONCLUSIONS

6.1 Summary and implications

The outcrop exposures of the Cloridorme Formation offer a rare opportunity to make detailed observations of the lateral continuity of event beds and elements of a basin plain depositional environment. A summary of key conclusions is provided below:

1. Sandstone beds in this region of the Cloridorme Formation display significant lateral heterogeneity in bed thickness, despite being described as sheet-like and bed correlations ranging in the tens of km. The bed-scale heterogeneity we observe highlights how submarine gravity flows themselves as well as their deposition (turbidites and hybrid event beds) are more complex than is commonly reported in basin plain environments. We propose four primary mechanisms responsible for the variations in bed geometries and interpret that many of the sandstone beds were influenced by seafloor topography and active tectonism during/shortly after deposition.

2. The vertical distribution of metrics such as N:G, AR, bed thickness, bed and element thinning rate, facies proportion, etc. were calculated and compared from element-to-element as well as laterally between measured sections. Downcurrent trends and short-scale lateral variations were observed in all of these metrics. Further statistical analysis of these data as well as more high-resolution bed-scale data from other outcrops is necessary.

3. Distal portions of basin plain systems do not follow simplistic, unidirectional trends away from an axis but instead display a pattern in which N:G, bed thickness, thinning rate, etc. transition away from locations of maximum sandiness in an irregular manner. This may be related to the compounded effect of irregularly-distributed sandstone beds and the influence of the basin floor and degree of confinement. Understanding the spatial scale at which these characteristics impact lateral heterogeneity is crucial for predicting the mechanical properties of a reservoir in horizontal drilling situations.

4. The stratigraphic completeness across the study area is relatively consistent, indicating up to 82.35% completeness. From this we can infer that almost one-fifth of flows do not preserve sandstone in this type of moderately confined basin plain environment, which implies there is still a fair amount of energy reworking the sediment in more distal locations. While many studies make bed-scale correlations in outcrops, it is also common practice to ignore or simply not correlate seemingly insignificant thin beds that likely pinch out over some distance. Because the methodology we use to calculate stratigraphic completeness is easy to replicate, we recommend it as a potentially useful metric for interpreting relative energy levels, and that more attention should be paid to correlating thin beds in order to more fully understand the range of flow processes present in different submarine environments.

5. Our analyses comparing beds laterally at high-resolution (1-m scale) highlight how important it is to recognize the potential effects of long-distance correlations when it comes to calculating key metrics such as thinning rate. We find that by averaging thinning rates over tens-to-hundreds of meters, the high degree of lateral variability that exists within the Cloridorme Formation at the bed scale is lost. This significantly impacts

the overall interpretation of the depositional environment and active flow processes. By measuring beds at as little as 1-m intervals, we produce thinning/thickening rates up to two orders of magnitude greater than those calculated from measured section correlations alone. We compare our results to previous works in the Cloridorme Formation and find that high resolution (1-m) measurements reveal that bed thinning rates are much higher than previously measured. Meanwhile, observed bed continuity and bed thickness appear in-line with other studies, despite the increased resolution of this study. From an industry perspective, lateral thickness variability at the bed-scale is difficult to discern. Therefore, predictive models of reservoir properties rely heavily on outcrop analogs as ground-truths for reproducing realistic flow processes and ultimately bed-scale heterogeneity. This study demonstrates the need for more high-resolution studies focusing on vertical and lateral bed-scale relationships to update current conceptual models of basin plain environments.

REFERENCES

Amy, L. A., and P. J. Talling, 2006, Anatomy of turbidites and linked debrites based on long distance (120 × 30 km) bed correlation, Marnoso Arenacea Formation, Northern Apennines, Italy: Sedimentology, v. 53, no. 1, p. 161–212, doi:10.1111/j.1365-3091.2005.00756.x.

Awadallah, S. A. M., and R. N. Hiscott, 2004, High-resolution stratigraphy of the deep-water lower Cloridorme Formation (Ordovician), Gaspé Peninsula, based on K-bentonite and megaturbidite correlations: Canadian Journal of Earth Sciences, v. 41, no. 11, p. 1299–1317, doi:10.1139/e04-078.

Baker, M. L., and J. H. Baas, 2020, Mixed sand–mud bedforms produced by transient turbulent flows in the fringe of submarine fans: Indicators of flow transformation: Sedimentology, v. 67, no. 5, p. 2645–2671, doi:10.1111/sed.12714.

Basu, D., and A. H. Bouma, 2000, Thin-bedded turbidites of the Tanqua Karoo: physical and depositional characteristics, *in* A. H. Bouma, and C. G. Stone, eds., Fine-grained turbidite systems: Tulsa, OK, American Association of Petroleum Geologists and SEPM (Society for Sedimentary Geology), p. 263–278, doi:10.1306/M72703C23.

Beeden, D. R., 1983, Sedimentology of Some Turbidites and Related Rocks from the Cloridorme Group, Ordovician, Quebec: McMaster University, Hamilton, Canada.

Bouma, A. H., 1962, Sedimentology of some Flysch deposits; a graphic approach to facies interpretation.: Amsterdam, Elsevier Publishing Company, 168 p.

Carlson, J., and J. P. Grotzinger, 2001, Submarine fan environment inferred from turbidite thickness distributions: Sedimentology, v. 48, no. 6, p. 1331–1351, doi:10.1046/j.1365-3091.2001.00426.x.

Cheng, C., and A. P. Bunger, 2019, Model-Based Evaluation of Methods for Maximizing Efficiency and Effectiveness of Hydraulic Fracture Stimulation of Horizontal Wells: Geophysical Research Letters, v. 46, no. 22, p. 12870–12880, doi:10.1029/2019GL084809.

Dall'Olio, E., F. Felletti, and G. Muttoni, 2013, Magnetic-fabric analysis as a tool to constrain mechanisms of deep-water mudstone deposition in the Marnoso Arenacea Formation (Miocene, Italy): Journal of Sedimentary Research, v. 83, no. 2, p. 170–182, doi:10.2110/jsr.2013.12.

Dennielou, B., A. Huchon, C. Beaudouin, and S. Berné, 2006, Vertical grain-size variability within a turbidite levee: Autocyclicity or allocyclicity? A case study from the Rhône neofan, Gulf of Lions, Western Mediterranean: Marine Geology, v. 234, no. 1–4, p. 191–213, doi:10.1016/j.margeo.2006.09.019.

Deptuck, M. E., D. J. W. Piper, B. Savoye, and A. Gervais, 2008, Dimensions and architecture of late Pleistocene submarine lobes off the northern margin of East Corsica: Sedimentology, v. 55, no. 4, p. 869–898, doi:10.1111/j.1365-3091.2007.00926.x.

Durkin, P. R., S. M. Hubbard, J. Holbrook, and R. Boyd, 2018, Evolution of fluvial meander-belt deposits and implications for the completeness of the stratigraphic record: Bulletin of the Geological Society of America, v. 130, no. 5–6, p. 721–739, doi:10.1130/B31699.1.

Enos, P., 1965, Anatomy of a Flysch: Cloridorme Formation (Middle Ordovician) Northern Gaspé Peninsula, Quebec: Yale University.

Enos, P., 1969a, Anatomy of a flysch: Journal of Sedimentary Research, v. 39, no. 2, p. 680–723, doi:10.1306/74D71CF8-2B21-11D7-8648000102C1865D.

Enos, P., 1969b, Cloridorme Formation, Middle Ordovician Flysch, Northern Gaspé Peninsula, Quebec: Special Paper of the Geological Society of America, v. 117, p. 1–61, doi:10.1130/SPE117-p1.

Fonnesu, M., P. Haughton, F. Felletti, and W. McCaffrey, 2015, Short length-scale variability of hybrid event beds and its applied significance: Marine and Petroleum Geology, v. 67, p. 583–603, doi:10.1016/j.marpetgeo.2015.03.028.

Fortey, R. A., D. A. T. Harper, J. K. Ingham, A. W. Owen, and A. W. A. Rushton, 1995, A revision of Ordovician series and stages from the historical type area: Geological Magazine, v. 132, no. 1, p. 15–30, doi:10.1017/S0016756800011390.

Fryer, R. C., and Z. R. Jobe, 2019, Quantification of the bed-scale architecture of submarine depositional environments: The Depositional Record, v. 5, no. 2, p. 192–211, doi:10.1002/dep2.70.

Fryer, R. C., Z. R. Jobe, F. Laugier, L. A. Pettinga, J. C. Gilbert, L. E. Shumaker, J. E. Smith, and M. Sullivan, 2021, Submarine lobe deposits of the Point Loma Formation, California: Quantifying event-bed architecture and lateral heterogeneity: Depositional Record, v. 7, no. 3, p. 374–391, doi:10.1002/dep2.156.

Haughton, P., C. Davis, W. McCaffrey, and S. Barker, 2009, Hybrid sediment gravity flow deposits - Classification, origin and significance: Marine and Petroleum Geology, v. 26, no. 10, p. 1900–1918, doi:10.1016/j.marpetgeo.2009.02.012.

Higley, D. K., M. P. Pantea, and R. M. Slatt, 1997, 3-D reservoir characterization of the House Creek oil field, Powder River Basin, Wyoming: Reston, VA, doi:10.3133/ds33.

Hiscott, R. N., K. T. Pickering, and D. R. Beeden, 1986, Progressive Filling of a Confined Middle Ordovician Foreland Basin Associated with the Taconic Orogeny, Quebec, Canada, *in* Foreland Basins: Oxford, UK, Blackwell Publishing Ltd., p. 307–325, doi:10.1002/9781444303810.ch17.

Hodgson, D. M., 2009, Distribution and origin of hybrid beds in sand-rich submarine fans of the Tanqua depocentre, Karoo Basin, South Africa: Marine and Petroleum Geology, v. 26, no. 10, p. 1940–1956, doi:10.1016/j.marpetgeo.2009.02.011.

Hubbard, S. M., Z. R. Jobe, B. W. Romans, J. A. Covault, Z. Sylvester, and A. Fildani, 2020,

The stratigraphic evolution of a submarine channel: Linking seafloor dynamics to depositional products: Journal of Sedimentary Research, v. 90, no. 7, p. 673–686, doi:10.2110/jsr.2020.36.

Islam, S., R. Hesse, and A. Chagnon, 1982, Zonation of diagenesis and low grade metamorphism in Cambro-Ordovician Flysche of Gaspe Peninsula, Quebec Appalachians: Canadian Mineralogist.

Jackson, A., A. Jackson, L. Stright, S. M. Hubbard, and B. W. Romans, 2019, Static connectivity of stacked deep-water channel elements constrained by high-resolution digital outcrop models: AAPG Bulletin, v. 103, no. 12, p. 2943–2973, doi:10.1306/03061917346.

Jobe, Z. R., N. Howes, J. Martin, R. Meyer, D. Coutts, P. Hou, L. Stright, and F. Laugier, 2021, Sedimentary graphic logs: A template for description and a toolkit for digitalization: The Sedimentary Record, v. 19, no. 3, p. 15–29, doi:10.2110/sedred.2021.3.3.

Jobe, Z. R., N. Howes, B. W. Romans, J. A. Covault, and C. R. Zane Jobe, 2018, Volume and recurrence of submarine-fan-building turbidity currents: The Depositional Record, v. 4, no. 2, p. 160–176, doi:10.1002/dep2.42.

St. Julien, P., and C. Hubert, 1975, Evolution of the Taconian Orogen in the Quebec Appalachians: American Journal of Science, v. 275, no. A, p. 337–362.

Kane, I. A., A. S. M. Pontén, B. Vangdal, J. T. Eggenhuisen, D. M. Hodgson, and Y. T. Spychala, 2017, The stratigraphic record and processes of turbidity current transformation across deep-marine lobes: Sedimentology, v. 64, no. 5, p. 1236–1273, doi:10.1111/sed.12346.

Kus, K. B., Z. R. Jobe, F. Laugier, W. Walker, and M. Sullivan, 2021, Quantifying the lateral heterogeneity of distal submarine lobe deposits, Point Loma Formation, California: Implications for subsurface lateral facies prediction: The Depositional Record, no. October, p. 1–30, doi:10.1002/dep2.169.

Kvale, E. P., C. M. Bowie, C. Flenthrope, C. Mace, J. M. Parrish, B. Price, S. Anderson, and W. A. DiMichele, 2020, Facies variability within a mixed carbonate-siliciclastic sea-floor fan (upper Wolfcamp Formation, Permian, Delaware Basin, New Mexico): AAPG Bulletin, v. 104, no. 3, p. 525–563, doi:10.1306/06121917225.

Lowe, D. R., 1982, Sediment gravity flows: II. Depositional models with special reference to the deposits of high-density turbidity currents.: Journal of Sedimentary Petrology, v. 52, no. 1, p. 279–297, doi:10.1306/212f7f31-2b24-11d7-8648000102c1865d.

Lowe, D. R., M. Guy, and A. Palfrey, 2003, Facies of slurry-flow deposits, Britannia Formation (Lower Cretaceous), North Sea: Implications for flow evolution and deposit geometry: Sedimentology, v. 50, no. 1, p. 45–80, doi:10.1046/j.1365-3091.2003.00507.x.

Ma, C., 1996, Continuity of sandstone beds in the Ordovician Cloridorme Formation, Gaspé Peninsula, Quebec: Memorial University of Newfoundland.

Macdonald, H. A., J. Peakall, P. B. Wignall, and J. Best, 2011, Sedimentation in deep-sea lobe-elements: Implications for the origin of thickening-upward sequences: Journal of the Geological Society, v. 168, no. 2, p. 319–331, doi:10.1144/0016-76492010-036.

Malgesini, G., P. J. Talling, A. J. Hogg, D. Armitage, A. Goater, and F. Felletti, 2015, Quantitative analysis of submarine-flow deposit shape in the Marnoso-Arenacea formation: What is the signature of hindered settling from dense near-bed layers? Journal of Sedimentary Research, v. 85, no. 2, p. 170–191, doi:10.2110/jsr.2015.15.

Manchanda, R., E. C. Bryant, P. Bhardwaj, P. Cardiff, and M. M. Sharma, 2016, Strategies for effective stimulation of multiple perforation clusters in horizontal wells: SPE Production and Operations, v. 33, no. 3, p. 539–556, doi:10.2118/179126-pa.

Marini, M., F. Felletti, S. Milli, and M. Patacci, 2016, The thick-bedded tail of turbidite thickness distribution as a proxy for flow confinement: Examples from tertiary basins of central and northern Apennines (Italy): Sedimentary Geology, v. 341, p. 96–118, doi:10.1016/j.sedgeo.2016.05.006.

Meirovitz, C. D., L. Stright, S. M. Hubbard, and B. W. Romans, 2020, The influence of inter- and intra-channel architecture on deep-water turbidite reservoir performance: Petroleum Geoscience, v. 27, no. 2, doi:10.1144/petgeo2020-005.

Mutti, E., 1977, Distinctive thin-bedded turbidite facies and related depositional environments in the Eocene Hecho Group (South-central Pyrenees, Spain): Sedimentology, v. 24, p. 107–131, doi:10.1111/j.1365-3091.1977.tb00122.x.

Mutti, E., and W. R. Normark, 1987, Comparing Examples of Modern and Ancient Turbidite Systems: Problems and Concepts: Marine Clastic Sedimentology, p. 1–38, doi:10.1007/978-94-009-3241-8_1.

Parkash, B., 1970, Downcurrent Changes in Sedimentary Structures in Ordovician Turbidite Greywackes: Journal of Sedimentary Petrology, v. 40, no. 2, p. 572–590, doi:10.1017/CBO9781107415324.004.

Pickering, K. T., and R. N. Hiscott, 1985, Contained (Reflected) Turbidity Currents from the Middle Ordovician Cloridorme Formation, Quebec, Canada: An Alternative to the Antidune Hypothesis: Sedimentology, v. 32, no. 3, p. 373–394, doi:10.1002/9781444304473.ch6.

Pickering, K. T., and R. N. Hiscott, 1995, Foreland basin-floor turbidite system, Cloridorme Formation, Quebec, Canada: long-distance correlation in sheet turbidites, *in* Atlas of Deep Water Environments: doi:10.1007/978-94-011-1234-5_48.

Prave, A. R., L. G. Kessler, M. Malo, W. V. Bloechl, and J. Riva, 2000, Ordovician arc collision and foredeep evolution in the Gaspe Peninsula, Quebec: The Taconic Orogeny in Canada and its bearing on the Grampian Orogeny in Scotland: Journal of the Geological Society, doi:10.1144/jgs.157.2.393.

Prélat, A., D. M. Hodgson, and S. S. Flint, 2009, Evolution, architecture and hierarchy of

distributary deep-water deposits: a high-resolution outcrop investigation from the Permian Karoo Basin, South Africa: Sedimentology, v. 56, no. 7, p. 2132–2154, doi:10.1111/j.1365-3091.2009.01073.x.

Pyrcz, M. J., O. Catuneanu, and C. V. Deutsch, 2005, Stochastic surface-based modeling of turbidite lobes: American Association of Petroleum Geologists Bulletin, v. 89, no. 2, p. 177–191, doi:10.1306/09220403112.

Ricci Lucchi, F., and E. Valmori, 1980, Basin-wide turbidites in a Miocene, over-supplied deep-sea plain: a geometrical analysis: Sedimentology, v. 27, no. 3, p. 241–270, doi:10.1111/j.1365-3091.1980.tb01177.x.

Riva, J. F., 1968, Graptolite faunas from the Middle Ordovician of the Gaspé North Shore: Naturaliste Canadian, v. 95, p. 1379–1400.

Romans, B. W., S. M. Hubbard, and S. A. Graham, 2009, Stratigraphic evolution of an outcropping continental slope system, Tres Pasos Formation at Cerro Divisadero, Chile: Sedimentology, v. 56, no. 3, p. 737–764, doi:10.1111/j.1365-3091.2008.00995.x.

Rowley, D. B., and W. S. F. Kidd, 1981, Stratigraphic Relationships and Detrital Composition of the Medial Ordovician Flysch of Western New England: Implications for the Tectonic Evolution of the Taconic Orogeny: The Journal of Geology, v. 89, no. 2, p. 199–218, doi:10.1086/628580.

Sadler, P. . ., 1981, Sediment Accumulation Rates and the Completeness of Stratigraphic Sections Author (s): Peter M . Sadler Published by : The University of Chicago Press Stable URL : http://www.jstor.com/stable/30062397 REFERENCES Linked references are available on JSTOR: The Journal of Geology, v. 89, no. 5, p. 569–584.

Skipper, K., and S. B. Bhattacharjee, 1978, Backset bedding in turbidites; a further example from the Cloridorme Formation (Middle Ordovician), Gaspe, Quebec: Journal of Sedimentary Research, v. 48, no. 1, p. 193–210, doi:10.1306/212F742D-2B24-11D7-8648000102C1865D.

Skipper, K., and G. V. Middleton, 1975, The Sedimentary Structures and Depositional Mechanics of Certain Ordovician Turbidites, Cloridorme Formation, Gaspé Peninsula, Quebec: Canadian Journal of Earth Sciences, doi:10.1139/e75-171.

Slivitzky, A., G. Lachambre, and P. S. Julien, 1991, Synthèse géologique du Cambro-Ordovicien du nord de la Gaspésie.

Spychala, Y. T., J. T. Eggenhuisen, M. Tilston, and F. Pohl, 2020, The influence of basin setting and turbidity current properties on the dimensions of submarine lobe elements: Sedimentology, v. 67, p. 3471–3491, doi:10.1111/sed.12751.

Spychala, Y. T., D. M. Hodgson, A. Prélat, I. A. Kane, S. S. Flint, and N. P. Mountney, 2017, Frontal and lateral submarine lobe fringes: Comparing sedimentary facies, architecture and flow processes: Journal of Sedimentary Research, v. 87, no. 1, p. 75–96,

doi:10.2110/jsr.2017.2.

van Staal, C. R., 1994, Brunswick subduction complex in the Canadian Appalachians: Record of the Late Ordovician to Late Silurian collision between Laurentia and the Gander margin of Avalon: Tectonics, v. 13, no. 4, p. 946–962, doi:10.1029/93TC03604.

Stright, L., J. Stewart, K. Campion, and S. Graham, 2014, Geologic and seismic modeling of a coarse-grained deep-water channel reservoir analog (Black's Beach, La Jolla, California): AAPG Bulletin, v. 98, no. 4, p. 695–728, doi:10.1306/09121312211.

Sumner, E. J., P. J. Talling, and L. A. Amy, 2009, Deposits of flows transitional between turbidity current and debris flow: Geology, v. 37, no. 11, p. 991–994, doi:10.1130/G30059A.1.

Sumner, E. J., P. J. Talling, L. A. Amy, R. B. Wynn, C. J. Stevenson, and M. Frenz, 2012, Facies architecture of individual basin-plain turbidites: Comparison with existing models and implications for flow processes: Sedimentology, v. 59, no. 6, p. 1850–1887, doi:10.1111/j.1365-3091.2012.01329.x.

Sylvester, Z., 2007, Turbidite bed thickness distributions: Methods and pitfalls of analysis and modelling: Sedimentology, v. 54, no. 4, p. 847–870, doi:10.1111/j.1365-3091.2007.00863.x.

Sylvester, Z., and D. R. Lowe, 2004, Textural trends in turbidites and slurry beds from the Oligocene flysch of the East Carpathians, Romania: Sedimentology, v. 51, no. 5, p. 945–972, doi:10.1111/j.1365-3091.2004.00653.x.

Sylvester, Z., C. Pirmez, and A. Cantelli, 2011, A model of submarine channel-levee evolution based on channel trajectories: Implications for stratigraphic architecture: Marine and Petroleum Geology, v. 28, no. 3, p. 716–727, doi:10.1016/j.marpetgeo.2010.05.012.

Talling, P. J., 2013, Hybrid submarine flows comprising turbidity current and cohesive debris flow: Deposits, theoretical and experimental analyses, and generalized models: Geosphere, v. 9, no. 3, p. 460–488, doi:10.1130/GES00793.1.

Talling, P. J., D. G. Masson, E. J. Sumner, and G. Malgesini, 2012, Subaqueous sediment density flows: Depositional processes and deposit types: Sedimentology, v. 59, no. 7, p. 1937–2003, doi:10.1111/j.1365-3091.2012.01353.x.

Tőkés, L., and M. Patacci, 2018, Quantifying tabularity of turbidite beds and its relationship to the inferred degree of basin confinement: Marine and Petroleum Geology, v. 97, no. February, p. 659–671, doi:10.1016/j.marpetgeo.2018.06.012.

Tucker, R. D., T. E. Krogh, R. J. Ross, and S. H. Williams, 1990, Time-scale calibration by high-precision UPb zircon dating of interstratified volcanic ashes in the Ordovician and Lower Silurian stratotypes of Britain: Earth and Planetary Science Letters, v. 100, no. 1–3, p. 51–58, doi:10.1016/0012-821X(90)90175-W.

Tucker, R. D., and W. S. Mckerrow, 1995, Early Paleozoic chronology: a review in light of new U - Pb zircon ages from Newfoundland and Britain: v. 379, p. 368–379, doi:10.1139/e95-032.

Vendettuoli, D. et al., 2019, Daily bathymetric surveys document how stratigraphy is built and its extreme incompleteness in submarine channels: Earth and Planetary Science Letters, v. 515, p. 231–247, doi:10.1016/j.epsl.2019.03.033.